J. Fluid Mech. (2000), *vol.* 406, *pp.* 81–107. Printed in the United Kingdom

Reynolds number dependence of the small-scale structure of grid turbulence

By T. ZHOU AND R. A. ANTONIA

Department of Mechanical Engineering, University of Newcastle, N.S.W., 2308, Australia

(Received 31 August 1998 and in revised form 13 October 1999)

The small-scale structure of grid turbulence is studied primarily using data obtained with a transverse vorticity (ω_3) probe for values of the Taylor-microscale Reynolds number R_λ in the range 27–100. The measured spectra of the transverse vorticity component agree within $\pm 10\%$ with those calculated using the isotropic relation over nearly all wavenumbers. Scaling-range exponents of transverse velocity increments are appreciably smaller than exponents of longitudinal velocity increments. Only a small fraction of this difference can be attributed to the difference in intermittency between the locally averaged energy dissipation rate and enstrophy fluctuations. The anisotropy of turbulence structures in the scaling range, which reflects the small values of R_λ, is more likely to account for most of the difference. All four fourth-order rotational invariants I_α ($\alpha = 1$ to 4) proposed by Siggia (1981) were evaluated. For any particular value of α, the magnitude of the ratio I_α/I_1 is approximately constant, independently of R_λ. The implication is that the invariants are interdependent, at least in isotropic and quasi-Gaussian turbulence, so that only one power-law exponent may be sufficient to describe the R_λ dependence of all fourth-order velocity derivative moments in this type of flow. This contrasts with previous suggestions that at least two power-law exponents are needed, one for the rate of strain and the other for vorticity.

1. Introduction

Significant evidence has emerged over the last few years on the relative behaviour of the scaling exponents associated with moments of order p of the longitudinal velocity increments (in which the velocity is in the same direction as the separation) and the transverse increments (in which the velocity is transverse to the separation) when the separation r lies within the inertial range (IR), i.e. $\eta \ll r \ll L$, where $\eta \equiv (\nu^3/\langle\epsilon\rangle)^{1/4}$ is the Kolmogorov length scale, ν is the kinematic viscosity of the fluid, $\langle\epsilon\rangle$ is the mean energy dissipation rate and angular brackets denote time averaging; $L \equiv U_1 \int_0^{\tau_0} \rho_{u_1u_1}(\tau)\,\mathrm{d}\tau$ is the longitudinal integral length scale, $\rho_{u_1u_1}$ is the longitudinal velocity autocorrelation coefficient, τ is the time delay and τ_0 is the time at which the first zero crossing occurs. With some exceptions (Kahalerras, Malecot & Gagne 1996; Camussi *et al.* 1996; Noullez *et al.* 1997), the available data from experiments (e.g. Herweijer & van de Water 1995; Camussi & Benzi 1997; Pearson & Antonia 1997; Dhruva, Tsuji & Sreenivasan 1997) and numerical calculations (e.g. Chen *et al.* 1997*b*; Boratav & Pelz 1997; Grossmann, Lohse & Reeh 1997) indicate that $\zeta_{u_2}(p) < \zeta_{u_1}(p)$, where $\zeta_{u_1}(p)$ and $\zeta_{u_2}(p)$ are the scaling exponents for the pth-order longitudinal and transverse velocity increments in the IR. The magnitude of the inequality, which increases with p, almost certainly depends on a number of factors, e.g. the Reynolds number, the presence of the mean shear or the level of structural

organization of the flow, some of these being most likely interrelated. The Reynolds number may be the most dominant factor as there is evidence (e.g. Dhruva *et al.* 1997) that the inequality nearly disappears for high Reynolds number atmospheric surface layer.

Various explanations have been proposed for the inequality, perhaps the most popular one (e.g. Chen *et al.* 1997*a*; Boratav & Pelz 1997) tending to associate the longitudinal velocity increment with either the strain rate or the energy dissipation rate ϵ and the transverse velocity increment with the mean-square vorticity or enstrophy respectively. Chen *et al.* (1997*a*) proposed a modification to the refined similarity hypothesis (RSH) (Kolmogorov 1962, hereafter referred to as K62), which they called the refined similarity hypothesis for transverse velocity increments (RSHT). They found that RSH and RSHT were well supported by their DNS data, indicating the possible existence of two independent scaling groups, one related to the rate of strain and the other to the vorticity. If indeed independent scaling groups are required, then, as Dhruva *et al.* (1997) pointed out, a richer small-scale phenomenology than has hitherto been used will need to be introduced. On the other hand, L'vov & Procaccia (1996) and Nelkin (1999) have argued that the asymptotic scaling exponents of locally averaged dissipation rates and enstrophy should be the same when $R_\lambda \to \infty$. Using models based on cylindrical vortices, He *et al.* (1998) also showed that both the differences in exponents for locally averaged dissipation rate and enstrophy and the differences between longitudinal and transverse velocity increments will disappear in the limit of infinite Reynolds numbers, implying that the Reynolds number is the main contributor to the latter differences.

It was pointed out by Sreenivasan & Antonia (1997) that if RSH is valid, the intermittency in the IR is inseparable from that in the dissipative range (DR). In this context, it is not unreasonable to expect different quantities in the DR to exhibit different behaviours, for example different Reynolds number dependences. The idea that both the instantaneous energy dissipation rate ϵ and enstrophy ω^2 may exert different influences on moments of different velocity derivatives was implicit in the proposal put forward by Siggia (1981). Specifically, he showed that, for homogeneous isotropic turbulence, the fourth-order velocity derivative moments can be expressed in terms of four scalar quantities (rotational invariants) given by

$$\left.\begin{aligned} I_1 &= \langle (e^2)^2 \rangle, \\ I_2 &= \langle \omega^2 e^2 \rangle, \\ I_3 &= \langle \omega_i e_{ij} e_{jk} \omega_k \rangle, \\ I_4 &= \langle (\omega^2)^2 \rangle, \end{aligned}\right\} \tag{1.1}$$

where e_{ij} $[\equiv \frac{1}{2}(u_{i,j} + u_{j,i})]$ is the rate of strain, $e^2 \equiv \sum e_{ij}^2$, ω_i $(\equiv \epsilon_{ijk} u_{k,j}$, where ϵ_{ijk} is the alternating tensor and $u_{k,j} \equiv \partial u_k / \partial x_j)$ is the vorticity, ω^2 $(\equiv \omega_1^2 + \omega_2^2 + \omega_3^2)$ is the enstrophy. Siggia (1981) calculated I_α from data obtained in a 64^3 direct simulation of stationary, homogeneous and isotropic turbulence ($R_\lambda = 60$ to 90). Not surprisingly, the numerical values of I_α were significantly larger than the corresponding Gaussian values of $\frac{7}{5}$, 2, $\frac{2}{3}$ and $\frac{20}{34}$ for $\alpha = 1$ to 4 respectively after normalization by $\langle e^2 \rangle^2$. Kerr (1985) carried out simulations (up to 128^3 grid points with periodic boundary conditions in all three directions) of isotropic turbulence and calculated I_α over a range of the Taylor microscale Reynolds number R_λ $(\equiv \lambda u_1' / \nu$, where $\lambda = u_1' / \langle u_{1,1}^2 \rangle^{1/2}$ is the Taylor microscale and the prime denotes root mean square (r.m.s.) value). Over the range $28 \leqslant R_\lambda \leqslant 89$, I_1, I_2 and I_4 increased with R_λ in power-law fashion with

exponents, estimated with an uncertainty of ± 0.03, of 0.18, 0.29 and 0.37 respectively. These values seem to suggest that at least two distinct exponents are needed, one for the rate of strain and the other for vorticity, in support of the implication by Siggia (1981). However, Kerr (1985) also noted that one exponent may suffice when R_λ is sufficiently large. Both Siggia (1981) and Kerr (1985) emphasized that more will be learned about small-scale intermittency by determining I_α in a high-quality wind tunnel than by measuring only $\langle u_{1,1}^4 \rangle$ at ever higher R_λ.

The measurement of I_α is not straightforward since nine velocity derivatives need to be determined simultaneously. To our knowledge, only Tsinober, Kit & Dracos (1992) reported estimates of I_α (F_α in their paper) in grid turbulence ($R_\lambda \simeq 70$) and at two locations in a boundary layer using a 12-hot-wire vorticity probe. They found that their values of I_α for the grid turbulence agreed, within 20%, with the DNS values of Siggia (1981) and Kerr (1985). They also noted that their estimates of I_α were closer to the Gaussian values, attributing this to the presence of random noise in their experiments. It is difficult to judge the accuracy of these estimates, especially since the effect of the spatial resolution of the probe does not appear to have been considered. Grid turbulence results were presented at only one flow speed; strictly, this should have resulted in an approximately constant value of R_λ at a sufficient distance from the grid (say $x_1/M \gtrsim 30$, where M is the grid mesh size). The tabulated values of R_λ (table 2 of their paper) indicate appreciable fluctuations with x_1/M; also, at some x_1 locations, the expected isotropic equality $\langle \omega_1^2 \rangle = \langle \omega_2^2 \rangle = \langle \omega_3^2 \rangle$ is violated, possibly due, at least in part, to an imperfect spatial resolution of their hot-wire probe.

It would clearly be of interest to measure I_α and examine its R_λ dependence in flows where local isotropy is approximately satisfied. However, the experimental estimation of I_α via (1.1) is difficult. The difficulty is compounded when the spatial resolution of the probe is inadequate; there is, as yet, no suitable method for correcting velocity derivative moments of order higher than 2 for the effect of spatial resolution. The assumption of isotropy considerably simplifies the determination of I_α. Siggia (1981) noted that the four invariants in (1.1) can be related to fourth-order velocity derivative correlations that are readily measurable. For example, an X-probe will yield, with the help of Taylor's hypothesis, three independent components of the fourth-order velocity gradient tensor, namely

$$\left.\begin{aligned} F_1 &= \langle u_{1,1}^4 \rangle, \\ F_2 &= \langle u_{1,1}^2 u_{2,1}^2 \rangle, \\ F_3 &= \langle u_{2,1}^4 \rangle. \end{aligned}\right\} \tag{1.2}$$

These three parameters are related to I_α as follows (Siggia 1981):

$$\left.\begin{aligned} F_1 &= 4I_1/105, \\ F_2 &= I_1/105 + I_2/70 - I_3/105, \\ F_3 &= 3I_1/140 + 11I_2/140 - 3I_3/35 + I_4/80. \end{aligned}\right\} \tag{1.3}$$

Using isotropy,

$$I_4 = 5\langle \omega_1^4 \rangle = 5\langle \omega_2^4 \rangle = 5\langle \omega_3^4 \rangle. \tag{1.4}$$

I_4 can be directly obtained from a one-component vorticity measurement. Once I_4 is known, (1.3) can be solved for I_1, I_2 and I_3.

In the present study, the I_α are estimated via (1.2)–(1.4) from data obtained primarily

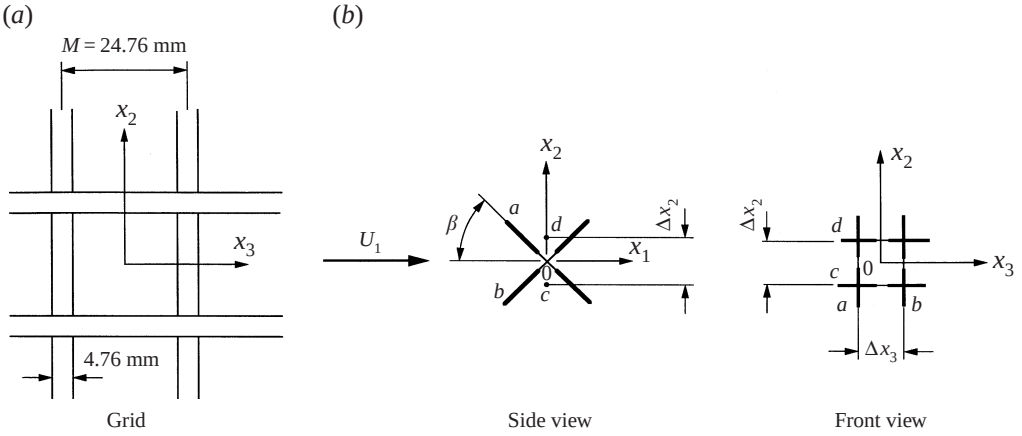

FIGURE 1. Sketches of (*a*) turbulence-generating grid and (*b*) lateral vorticity probe.

with a one-component vorticity (ω_3) probe in grid turbulence. These estimates are compared with those inferred from (1.1). This comparison is possible because of data previously obtained in the same flow using a four-X-wire three-dimensional vorticity probe, though at only one value of R_λ (experimental details can be found in Antonia, Zhou & Zhu 1998). The present measurements are obtained over a sufficient R_λ range to permit the R_λ dependences of various fourth-order velocity derivative moments to be compared with those obtained from numerical simulations (e.g. Siggia 1981; Kerr 1985) and experiments (e.g. Tsinober *et al.* 1992). It also allows the relative R_λ dependences of $\zeta_{u_1}(p)$ and $\zeta_{u_2}(p)$ to be examined.

Grid turbulence was chosen primarily because it provides a reasonably close approximation to isotropic turbulence, thus allowing a comparison with results from available periodic-box turbulence simulations. A significant advantage of this flow is that it allows the accuracy of the measurement technique to be checked since the measured mean turbulent energy dissipation rate can be compared with that estimated, with relatively good accuracy, from the streamwise decay rate of the mean turbulent energy.

2. Experimental details

Measurements of ω_3 were made on the centreline of the working section (350 mm × 350 mm, 2.4 m long) of a non-return blower-type low-turbulence wind tunnel. The measurement location was at $x_1/M = 70$ (where M is the mesh size of the grid) downstream of a biplane grid placed at the entrance to the working section. A square mesh ($M = 24.76$ mm with 4.76 mm × 4.76 mm square rods) grid with a solidity of 0.35 was used. A definition sketch of the grid and the coordinate system is shown in figure 1(*a*). The mean velocity U_1 was varied between 3 m s^{-1} and 21.2 m s^{-1}. The corresponding variation in the Taylor microscale Reynolds number R_λ was 27 to 100 (see table 1).

The transverse vorticity ω_3 was obtained using a four-hot-wire vorticity probe sketched in figure 1(*b*). This probe consisted of a pair of parallel wires c and d straddling wires a and b of an X-probe. The quantity ω_3 was approximated by

$$\omega_3 = \frac{\Delta u_2}{\Delta x_1} - \frac{\Delta u_1}{\Delta x_2} = -U_1^{-1}\frac{\Delta u_2}{\Delta t} - \frac{\Delta u_1}{\Delta x_2}, \tag{2.1}$$

U_1		λ	η	f_c	f_K	f_s			$\langle\epsilon\rangle$	L	u_1'	u_2'
(m s^{-1})	R_λ	(mm)	(mm)	(kHz)	(kHz)	(kHz)	Δx_2^*	Δx_3^*	(m^2 s^{-3})	(mm)	(cm s^{-1})	(cm s^{-1})
3	27	9.25	0.90	0.63	0.53	1.89	1.5	1.5	0.006	22.1	4.6	4.1
4.8	50	8.14	0.58	1.6	1.32	3.2	1.6	2.1	0.032	55.2	9.6	7.1
7.6	62	6.5	0.42	3.15	2.94	6.3	2.2	2.9	0.12	45.7	15	11.4
11.3	75	5.36	0.30	6.3	5.85	12.6	2.0	2.7	0.4	42.1	22	17.4
14.1	83	4.64	0.26	8.0	8.52	16.0	2.3	3.2	0.83	42.5	27.5	21.8
16.9	89	4.08	0.24	12.5	11.4	25.0	2.5	3.4	1.37	38.1	32.5	25
21.2	100	3.81	0.20	16.0	16.8	32.0	3.0	4.1	2.56	42.4	40	31.4

$R_\lambda \equiv u_1'\lambda/\nu$ is the Taylor microscale Reynolds number.
$\lambda \equiv u_1'/\langle u_{1,1}^2\rangle^{1/2}$ is the longitudinal Taylor microscale.
$\eta \equiv \nu^{3/4}/\langle\epsilon\rangle^{1/4}$ is the Kolmogorov length scale.
f_c and f_s are the cut-off frequency and sampling frequency respectively.
$f_K \equiv U_1/(2\pi\eta)$ is the Kolmogorov frequency.
$L \equiv U_1 \int_0^{\tau_0} \rho_{u_1 u_1}(\tau)\,\mathrm{d}\tau$ is the longitudinal integral length scale.

TABLE 1. Summary of experimental conditions for transverse vorticity measurement at $x_1/M = 70$.

where Δu_1 is the difference between the longitudinal velocity fluctuations from two parallel hot wires which are separated in the x_2-direction; Δu_2 is the difference between values of u_2 at the same point in space but separated in time by one sampling time interval Δt ($\approx f_s^{-1}$; f_s is the sampling frequency). Because the turbulence intensity is small ($u_i'/U_1 \leqslant 2\%$, $i = 1, 2, 3$), the use of Taylor's hypothesis, i.e. $\Delta/\Delta x_1 = -U_1^{-1}\Delta/\Delta t$ in (2.1), should be satisfactory. A forward differencing scheme was used to convert temporal to spatial derivatives, the magnitude of Δx_1 being approximately equal to that of Δx_2.

Three vorticity probes with different wire separations (see table 1) were used. The separation Δx_2 was adjusted before the wires were etched so that Δx_2^* (the superscript $*$ denotes normalization by the Kolmogorov length scale η and/or the Kolmogorov velocity scale $U_K \equiv (\nu\langle\epsilon\rangle)^{1/4}$) remained in the range of 2 to 4 (e.g. Antonia, Zhu & Kim 1993; Zhu & Antonia 1995). This strategy was adopted to try to minimize any noise contamination due to too small a separation and any spectral attenuation due to too large a separation. These two effects can adversely influence the quality of the measured fourth-order velocity derivative correlations. The decay of the mean turbulent energy $\langle q^2\rangle$ ($\equiv \langle u_1^2\rangle + \langle u_2^2\rangle + \langle u_3^2\rangle$) in the longitudinal direction was measured with a probe comprising two X-wires. The X-wires were arranged orthogonally, one in the (x_1, x_2)- and the other in the (x_1, x_3)-plane; in this way, all three components of the velocity fluctuation vector were determined simultaneously. The wire separation in each X-wire was about 0.8 mm, corresponding to 3.7η–1.6η (for $x_1/M = 20$–80). This measurement was made for $U_1 = 7\,\mathrm{m\,s^{-1}}$ at seven locations ($x_1/M = 20$ to 80) along the tunnel. The included angles for the X-wire in the one-component vorticity probe and the two X-wire probe were about 100°, large enough to minimize the effect of large velocity cone angles (e.g. Browne, Antonia & Chua 1989). All probes comprised 2.5 μm diameter Wollaston Pt–10% Rh wires, each etched to an active length of about 0.5 mm. The length to diameter ratio of the wire was about 200.

Velocity components measured with X-wires can be significantly in error when velocity gradients are large (e.g. Vukoslavcevic & Wallace 1981; Kawall, Shokr & Keffer 1983; Hirota, Fujita & Yokosawa 1988; Park & Wallace 1993; Zhu & Antonia

1995). The mean velocity gradient is zero in the present flow. We estimated that the errors in u_1', u_2' and u_3' arising from the instantaneous velocity gradient fluctuations could be no greater than 3%. The effect of the cross-stream velocity on the X-wire was neglected because of the low turbulence intensity ($< 2\%$ for all R_λ).

Experimental uncertainties were estimated for all measured quantities. In the case of U_1 and u_i ($i = 1, 2$), estimates were inferred from errors in the hot-wire calibration data as well as from the scatter (20 to 1 odds) observed in repeating the experiment a number of times. The uncertainty in U_1 was about $\pm 2\%$. The uncertainties in u_1' and u_2' were about $\pm 5\%$. Uncertainties in the separations Δx_1 and Δx_2 were $\pm 2\%$ and $\pm 5\%$ respectively. Using the previous estimates, uncertainties for other quantities were estimated by the method of propagation of errors (e.g. Moffat 1988).

The hot wires were operated with in-house constant-temperature circuits at an overheat ratio of 1.5. Output signals from the anemometers were passed through buck-and-gain circuits and low-pass filtered at a cut-off frequency f_c (see table 1). f_c was chosen after examining the spectrum of $\partial u_1/\partial t$ and identifying the onset of electronic noise (the procedure was similar to that outlined in Antonia, Satyaprakash & Hussain 1982). The values of f_c were generally close to $U_1/2\pi\eta$, which is commonly identified as the Kolmogorov frequency f_K. The filtered signals were then sampled at a frequency of $f_s \simeq 2f_c$ into a PC (IBM compatible Pentium 70) using a 12 bit A/D converter. The number of samples for each channel was 2.1×10^6 to ensure convergence of the highest-order ($p = 8$) moments of the velocity increments. The convergence criteria proposed by Anselmet *et al.* (1984) and Camussi & Guj (1996) were satisfied.

3. Anisotropy of velocity and vorticity fluctuations

As noted earlier, grid turbulence was chosen partly because the performance of the vorticity probe can be checked and mainly because the flow provides a reasonable approximation to homogeneous and isotropic turbulence. A few local isotropy checks were made by Antonia *et al.* (1998) in the same grid flow at $R_\lambda = 45$. We consider here the possible influence of R_λ on local isotropy.

A measure of anisotropy of velocity and vorticity fluctuations is provided by the ratio of the spectra calculated using isotropy and the measured spectra. The measured spectra were first corrected for the effect of wire separation and wire length. The correction procedure has been outlined in detail in Zhu & Antonia (1995) and Antonia, Zhu & Shafi (1996). For isotropic turbulence, because of the solenoidality of u_i in an incompressible flow (e.g. Monin & Yaglom 1975; Antonia & Kim 1994), the spectrum $\phi_{u_2}(k_1)$ or $\phi_{u_3}(k_1)$ can be written in terms of $\phi_{u_1}(k_1)$:

$$\phi_{u_2}(k_1) = \phi_{u_3}(k_1) = \frac{1}{2}\left(1 - k_1\frac{\partial}{\partial k_1}\right)\phi_{u_1}(k_1). \tag{3.1}$$

The spectral density ϕ_α^* is defined such that $\int_0^\infty \phi_\alpha^*(k_1^*)\,\mathrm{d}k_1^* = \langle \alpha^{*2}\rangle$ ($\alpha = u_1, u_2, u_3$ and ω_3). Measured distributions of $\phi_{u_1}^*$ were used as input when (3.1) was implemented. When isotropy is satisfied, the ratio $\phi_{u_2}^{*c}/\phi_{u_2}^{*m}$ (the superscript c denotes the calculated spectrum using (3.1) and the superscript m denotes the measured and corrected spectrum) should be 1 (e.g. Kim & Antonia 1993; Saddoughi & Veeravalli 1994). Figure 2 shows this ratio for several values of R_λ (to avoid crowding, only results for $R_\lambda = 27$, 62, 83 and 100 are shown; this also applies to figure 3). The ratio is as large as 1.2 for $k_1^* > 0.1$. The rise at lower wavenumbers reflects the increasing

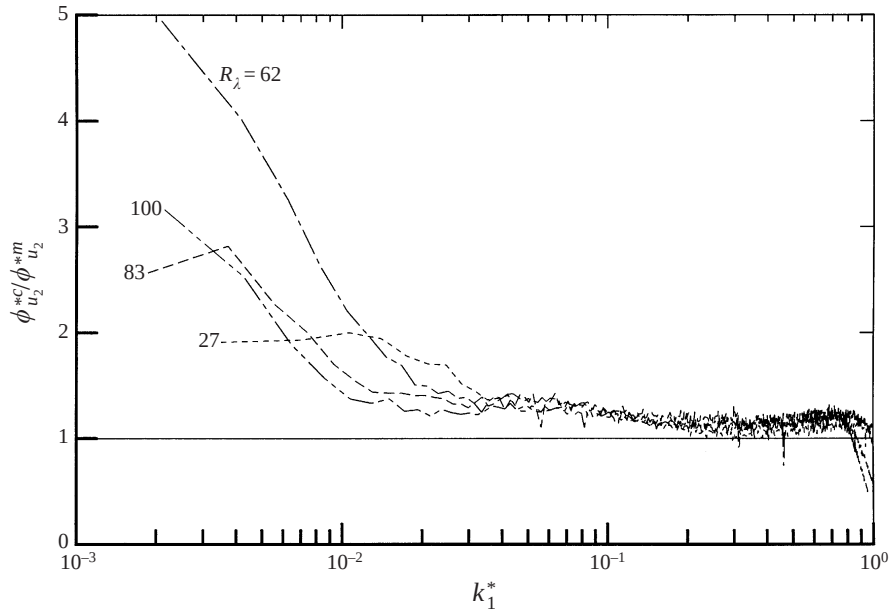

FIGURE 2. Ratios of calculated and measured spectra of u_2 for different Reynolds numbers. The calculation, (3.1), is based on isotropy. - - -, $R_\lambda = 27$; — - —, 62; – –, 83; — - - —, 100. The solid line indicates the isotropic value of 1.

anisotropy as the scale increases. Indeed, the present values of $\langle u_1^2 \rangle$ and $\langle u_2^2 \rangle$ show large departures from isotropy, the ratio $\langle u_1^2 \rangle / \langle u_2^2 \rangle$ being approximately equal to 1.7 at all values of R_λ. The ratio falls below 1 for $k_1^* > 0.8$ due mainly to the noise contamination of the spectra.

Assuming isotropy, $\phi_{\omega_2}(k_1)$ or $\phi_{\omega_3}(k_1)$ can be written as (e.g. Van Atta 1991; Kim & Antonia 1993)

$$\phi_{\omega_2}(k_1) = \phi_{\omega_3}(k_1) = \tfrac{5}{2}\phi_{u_{1,1}}(k_1) - \frac{k_1}{2}\frac{\partial \phi_{u_{1,1}}(k_1)}{\partial k_1} + 2\int_{k_1}^{\infty} \frac{\phi_{u_{1,1}}(k)}{k}\,\mathrm{d}k. \tag{3.2}$$

Unlike the ratio $\phi^{*c}_{u_2}/\phi^{*m}_{u_2}$ shown in figure 2, the ratio $\phi^{*c}_{\omega_3}/\phi^{*m}_{\omega_3}$ (figure 3) is close to 1 (within $\pm 10\%$) for $k_1^* \leqslant 0.8$, independently of R_λ. The decrease of the ratio for $k_1^* > 0.8$ is due mainly to noise contamination. This behaviour is consistent with Antonia & Kim's (1994) conclusion that isotropy is satisfied, almost independently of R_λ, provided k_1^* is sufficiently large and the Kolmogorov-normalized mean shear is suitably small (here the mean shear is zero).

The anisotropy can also be assessed by examining the departures of the measured second-order moments from the isotropic relations

$$\left.\begin{aligned} \langle \omega_1^2 \rangle = \langle \omega_2^2 \rangle = \langle \omega_3^2 \rangle &= 5\langle u_{1,1}^2 \rangle, \\ \langle u_{1,2}^2 \rangle = \langle u_{2,1}^2 \rangle = \langle u_{1,3}^2 \rangle = \langle u_{3,1}^2 \rangle = \langle u_{2,3}^2 \rangle = \langle u_{3,2}^2 \rangle &= 2\langle u_{1,1}^2 \rangle, \\ -\langle u_{1,2}u_{2,1} \rangle = -\langle u_{1,3}u_{3,1} \rangle = -\langle u_{2,3}u_{3,2} \rangle &= \tfrac{1}{2}\langle u_{1,1}^2 \rangle. \end{aligned}\right\} \tag{3.3}$$

Figure 4 shows the corrected second-order moments of ω_3 and its components, normalized by $\langle u_{1,1}^2 \rangle$ against R_λ. For $\langle u_{1,2}^2 \rangle$ and $-\langle u_{1,2}u_{2,1} \rangle$, the departure is within $\pm 5\%$. The departure (–10%) is bigger for $\langle \omega_3^2 \rangle$ mainly due to the departure (–15%) of $\langle u_{2,1}^2 \rangle$ from isotropy. All of these departures seem to be independent of R_λ.

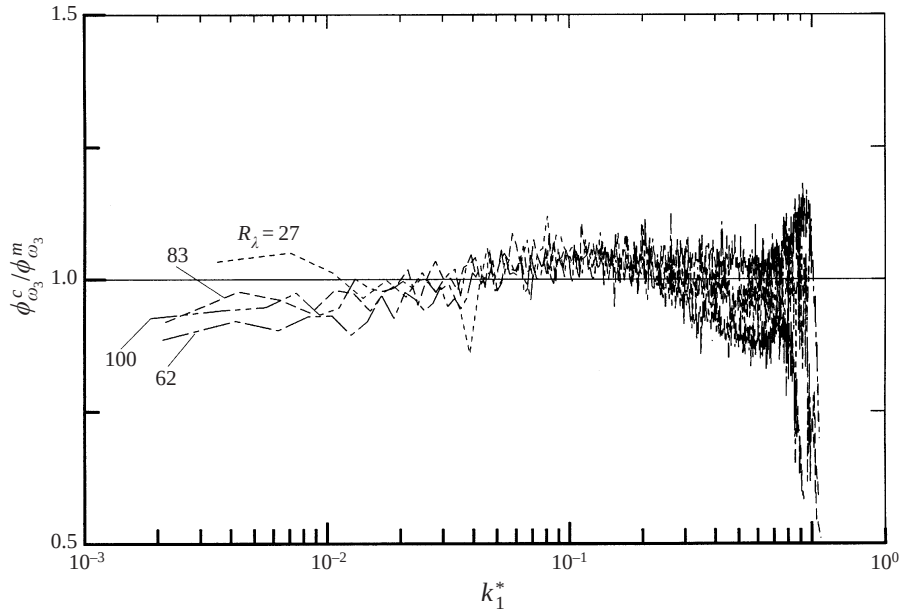

FIGURE 3. Ratios of calculated and measured spectra of ω_3 for different Reynolds numbers. The calculation, (3.2), is based on isotropy. - - -, $R_\lambda = 27$; — - —, 62; – –, 83; — - - —, 100. The solid line indicates the isotropic value of 1.

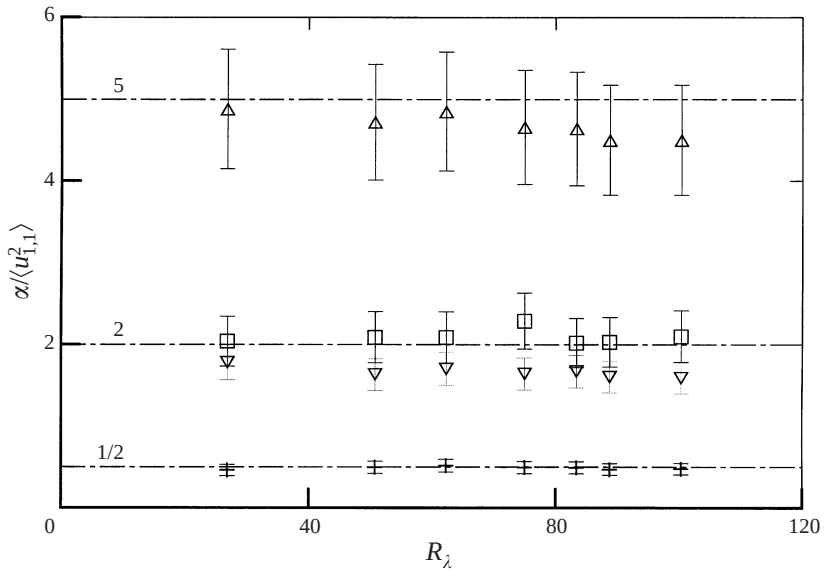

FIGURE 4. R_λ dependence of the variance of ω_3 and of its components. Each quantity is normalized by $\langle u_{1,1}^2 \rangle$. Isotropic values are indicated by horizontal lines. △, $\alpha = \langle \omega_3^2 \rangle$; □, $\langle u_{1,2}^2 \rangle$; ▽, $\langle u_{2,1}^2 \rangle$ +, $-\langle u_{1,2} u_{2,1} \rangle$. Error bars indicate experimental uncertainties.

In grid turbulence, the mean turbulent energy dissipation rate $\langle \epsilon \rangle$ can be determined with relatively good accuracy from the rate of decay of the mean turbulent energy in a region where homogeneity and isotropy are approximately satisfied (e.g. Mohamed & LaRue 1990). Assuming homogeneity and isotropy, the transport equation for the

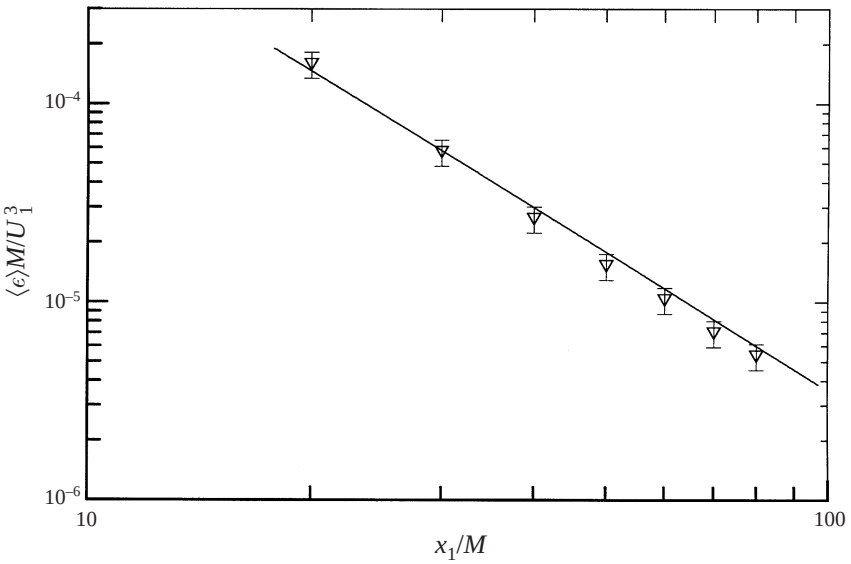

FIGURE 5. Comparison of the mean energy dissipation rate $\langle\epsilon\rangle$ obtained from the measured decay rate of the mean turbulent energy with its isotropic value for $R_\lambda = 60$. —, Obtained from (3.4); ∇, $\langle\epsilon\rangle_{iso}$. Error bars indicate experimental uncertainties.

mean turbulent energy $\langle q^2\rangle \equiv \langle u_i u_i\rangle$ simplifies to

$$-U_1 \frac{\mathrm{d}}{\mathrm{d}x_1}(\tfrac{1}{2}\langle q^2\rangle) = \langle\epsilon\rangle. \tag{3.4}$$

The comparison between $\langle\epsilon\rangle$, obtained from (3.4), and the isotropic value $\langle\epsilon\rangle_{iso} = 15\nu\langle u_{1,1}^2\rangle$ is a direct check of local isotropy. In figure 5, values of $\langle\epsilon\rangle$ are compared with $\langle\epsilon\rangle_{iso}$ for $R_\lambda = 60$. The agreement, always better than $\pm 15\%$, is comparable to that indicated in figures 2 and 3.

The streamwise rate of change of ω_3' can also be checked against the relation (Batchelor & Townsend 1947)

$$U_1 \frac{\mathrm{d}(1/\omega_3')}{\mathrm{d}x_1} = \frac{7}{6\sqrt{5}}\left(S + \frac{2G}{R_\lambda}\right), \tag{3.5}$$

where $S \equiv \langle u_{1,1}^3\rangle / \langle u_{1,1}^2\rangle^{3/2}$ is the skewness of $u_{1,1}$ and $G \equiv \langle u_1^2\rangle \langle u_{1,11}^2\rangle / \langle u_{1,1}^2\rangle^2$ (note $u_{1,11} \equiv \partial^2 u_1/\partial x_1^2$; $\langle u_{1,11}^2\rangle$ is estimated using $\langle u_{1,11}^2\rangle = \int_0^\infty k_1^4 \phi_{u_1}(k_1)\,\mathrm{d}k_1$) can be interpreted as an enstrophy destruction coefficient. The skewness of $u_{1,1}$ is about -0.4 in the range $20 \leqslant x_1/M \leqslant 80$. Figure 6 indicates that the left and right sides of (3.5) agree within $\pm 15\%$.

4. R_λ dependence of second- and third-order moments of δu_1

Starting with the Kármán–Howarth (1938) equation, Kolmogorov (1941, hereafter referred to as K41) derived an equation relating $\langle(\delta u_1)^2\rangle$ and $\langle(\delta u_1)^3\rangle$ for homogeneous isotropic turbulence, namely

$$-\langle(\delta u_1)^3\rangle + 6\nu \frac{\partial}{\partial r}\langle(\delta u_1)^2\rangle = \tfrac{4}{5}\langle\epsilon\rangle r, \tag{4.1}$$

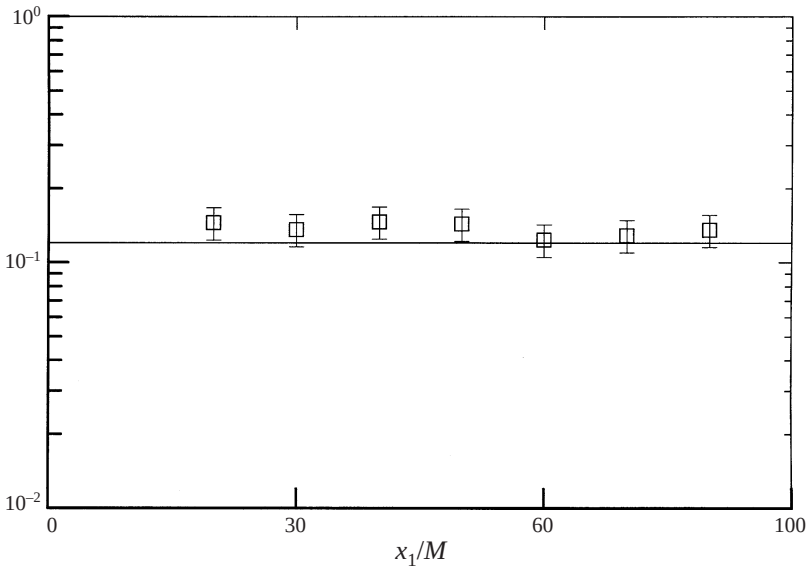

FIGURE 6. Comparison of terms on the left-hand (——) and right-hand (□) sides of (3.5). Error bars indicate experimental uncertainties.

where $\delta u_1 \equiv u_1(x_1 + r) - u_1(x_1)$ is the longitudinal velocity increment. In the IR, the second term of (4.1) should be negligible and (4.1) reduces to the so-called four-fifths law:

$$-\langle(\delta u_1)^3\rangle = \tfrac{4}{5}\langle\epsilon\rangle r. \tag{4.2}$$

The region where $\langle(\delta u_1)^3\rangle$ varies linearly with r is often identified with the IR.

In the DR,

$$\langle(\delta u_1)^2\rangle = \frac{1}{15\nu}\langle\epsilon\rangle r^2. \tag{4.3}$$

The present distributions of $-r^{*-1}\langle(\delta u_1^*)^3\rangle$ are shown in figure 7 together with the higher-R_λ data of Mydlarski & Warhaft (1996). The peak value of this quantity, here denoted by C_3, increases systematically with R_λ asymptotically approaching '$\frac{4}{5}$'. This approach suggests that it is unlikely that the scaling range satisfies isotropy before $R_\lambda \simeq 1000$; alternatively, it could be argued that a proper IR is unlikely to be established before this value is reached. A larger limiting value of R_λ would apply when a mean shear is present. In a recent paper by Danaila *et al.* (1999) (see also Lindborg 1999), a more general form of the Kolmogorov equation was written for decaying grid turbulence. A source term, reflecting the non-stationarity of the second-order velocity increment was included. This term closes the Kolmogorov equation quite well, despite the small value of R_λ, reflecting the non-negligible influence from the non-stationarity of the second-order velocity increments. Arguably, this additional term may also be interpreted as representing the non-homogeneity which arises from the streamwise decay of the energy originally injected in the flow at a scale ($\simeq M$) corresponding to that of the grid, i.e. M. One may also speculate that the non-negligible contribution of the source term reflects a lack of homogeneity and therefore a lack of isotropy in the scaling range. As R_λ increases, the influence from the source term on the scaling range decreases and the isotropy over this range improves, as reflected by the trend in figure 7.

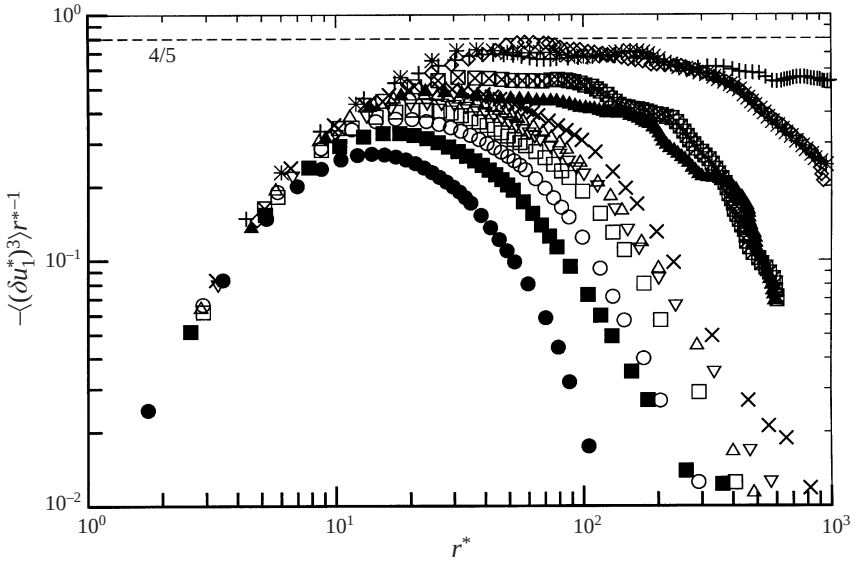

FIGURE 7. Third-order moments of δu_1^* multiplied by r^{*-1} for different Reynolds numbers and compared with higher R_λ values of Mydlarski & Warhaft (1996). Present: ●, $R_\lambda = 27$; ■, 50; ○, 62; □, 75; ▽, 83; △, 89; ×, 100. Mydlarski & Warhaft (1996): ▲, 99; ⊠, 134; ◇, 319; *, 448; +, 671. Equation (4.2): - - -.

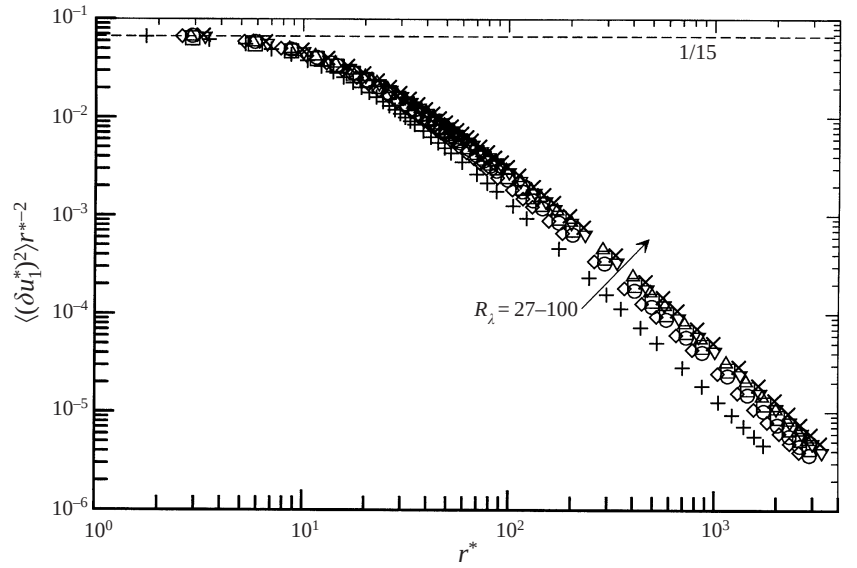

FIGURE 8. Dependence of $\langle(\delta u_1^*)^2\rangle r^{*-2}$ on R_λ. +, $R_\lambda = 27$; ◇, 50; ○, 62; □, 75; ▽, 83; △, 89; ×, 100; - - -, (4.3).

The second-order structure functions are shown in figure 8; $\langle(\delta u_1^*)^2\rangle$ is multiplied by r^{*-2} to allow the DR scales to be compared with local isotropy. At small r^*, $\langle(\delta u_1^*)^2\rangle r^{*-2}$ satisfies (4.3), independently of R_λ. This is consistent with the expectation that DR scales should approach isotropy more rapidly than IR scales. In the IR, the product $r^{*-2/3}\langle(\delta u_1^*)^2\rangle$, here denoted by C_2, is expected to become constant when

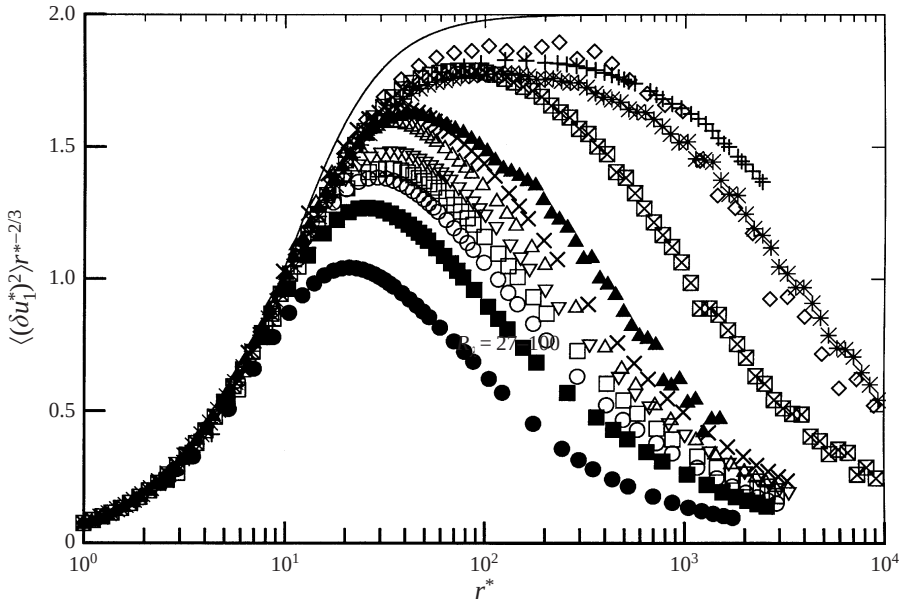

FIGURE 9. Second-order structure functions multiplied by $r^{*-2/3}$ and comparison with theoretical values and the higher-R_λ values of Mydlarski & Warhaft (1996). Present: ●, $R_\lambda = 27$; ■, 50; ○, 62; □, 75; ▽, 83; △, 89; ×, 100. Mydlarski & Warhaft (1996): ▲, 99; ⊠, 134; ◇, 319; *, 448; +, 671. Batchelor (equation (4.5)): —.

R_λ is sufficiently large. The data examined by Yaglom (1981) suggested that the magnitude of this constant is about 2, albeit with a fair degree of scatter. As in the case of $r^{*-1}\langle(\delta u_1^*)^3\rangle$ (figure 7), the present distributions of $r^{*-2/3}\langle(\delta u_1^*)^2\rangle$ (figure 9) do not exhibit a clear plateau. The peak magnitude of $r^{*-2/3}\langle(\delta u_1^*)^2\rangle$ increases systematically with R_λ. $C_2 \simeq 1.64$ at $R_\lambda = 100$; we estimate that $C_2 \simeq 1.65$ ($R_\lambda = 99$) for Mydlarski & Warhaft. No information on $\langle(\delta u_i)^2\rangle$ was presented by the previous authors; their u_1 spectra were converted to $\langle(\delta u_1)^2\rangle$ by applying the relation (e.g. Tatarskii 1971)

$$\langle(\delta u_i)^2\rangle = 2\int_0^\infty [1-\cos(k_1 r)]\phi_{u_i}(k_1)\,\mathrm{d}k_1, \tag{4.4}$$

where the subscript i equals 1, 2 and 3. The Mydlarski & Warhaft data indicate that $r^{*-2/3}\langle(\delta u_1^*)^2\rangle$ become flatter over the IR as R_λ increases. The magnitude of C_2 increases but the scatter, notwithstanding the relatively small uncertainty in estimating $\langle\epsilon\rangle$ in this flow, is sufficiently large to prevent any firm conclusion about the asymptotic value of C_2. Note that the solid line represents the 'asymptotic' distribution suggested by Batchelor (1951) for very high R_λ,

$$\langle(\delta u_1^*)^2\rangle = \frac{r^{*2}}{15[1+(15C_2)^{-3/2}r^{*2}]^{2/3}}, \tag{4.5}$$

with $C_2 = 2$. Clearly, even for the high R_λ data of Mydlarski & Warhaft ($R_\lambda = 671$), there is a large departure from the Batchelor distribution in the IR. Equation (4.5) was used in slightly different forms by a number of other investigators (e.g. Stolovitzky, Sreenivasan & Juneja 1993; Lohse & Müller-Groeling 1995) to account for the

crossover from the DR to IR. Stolovitzky *et al.* (1993) included an intermittency correction to (4.5), which can be written more generally as

$$\langle(\delta\beta^*)^2\rangle = \frac{a_\beta r^{*2}}{(1+b_\beta r^{*2})^{c_\beta}}, \tag{4.6}$$

where $\beta \equiv u_1$, u_2, u_3 and a_β, b_β, c_β may depend on R_λ; in particular c_β is related to the power-law exponent $\zeta_\beta(2)$ via $c_\beta = [2-\zeta_\beta(2)]/2$. The resulting expression for arbitrary-order structure functions, valid for dissipative as well as inertial range scales, was satisfactorily supported by their boundary layer data.

Two main comments need to be made with respect to figure 9.

(*a*) The information cannot be reconciled with the conclusion by Sreenivasan (1995) that the (spectral) Kolmogorov constant is 'more or less universal, essentially independent of the flow as well as the Reynolds number (for $R_\lambda > 50$ or so)'. The figure points to C_2 becoming constant only beyond a value of R_λ of roughly 1000. Mydlarski & Warhaft (1996) observed that both the spectral power-law exponent and the corresponding proportionality constant (C_{1*} in their paper) vary with R_λ. Their data suggest that the $-\frac{5}{3}$ spectral power-law exponent and the constant of 0.5 are not obtained before $R_\lambda \gtrsim 10^4$. The trial and error method adopted by Mydlarski & Warhaft for optimizing the scaling range could not be meaningfully implemented in our case, due to the small R_λ range of the present experiment.

(*b*) The R_λ dependence in figure 9 is however consistent with the R_λ dependence in figure 7. It seems that the anisotropy in the scaling range which affects C_3 also affects C_2.

5. R_λ dependence of scaling exponents

In the present study, transverse increments are identified with $\delta u_2 = u_2(x_1+r) - u_2(x_1)$. They can also be formed from differences in u_1 fluctuations separated in a direction transverse to the mean flow (e.g. Herweijer & van de Water 1995; Kahalleras *et al.* 1996; Noullez *et al.* 1997; Chen, Sreenivasan & Nelkin 1997*a*). This is not done here. The scaling exponents $\zeta_{u_1}(p)$ and $\zeta_{u_2}(p)$, namely $\langle(\delta u_1)^p\rangle \sim r^{\zeta_{u_1}(p)}$ and $\langle(\delta u_2)^p \sim r^{\zeta_{u_2}(p)}$ in the IR, were estimated using essentially the extended self-similarity (ESS) method proposed by Benzi *et al.* (1993) by plotting $\langle|\delta u_1|^p\rangle$ and $\langle|\delta u_2|^p\rangle$ against $\langle|\delta u_1|^3\rangle$. Unlike the ESS method, the scaling range was restricted to a range of r for which $r^{-1}\langle|\delta u_1|^3\rangle$ is nearly constant (figure 10). The plateau in $r^{-1}\langle|\delta u_1|^3\rangle$ is more extended than that in $r^{-1}\langle(\delta u_1)^3\rangle$. The claim by Benzi *et al.* (1993) that the scaling extends into the DR becomes tenuous as the magnitude of p increases. This is illustrated in figure 11(*a*) for $\langle|\delta u_1|^p\rangle$. It is more emphatic for $\langle|\delta u_2|^p\rangle$ (figure 11*b*). The curvature exhibited by figure 11(*b*) is not an artefact of the record duration, which was sufficiently long for the integrands $|\delta u_i|^p\ P_{|\delta u_i|}$ (where $P_{|\delta u_i|}$ is the probability density function of $|\delta u_i|$ with $i = 1$ and 2) to close for $p = 8$. It represents a genuine departure from the relatively linear behaviour exhibited by the third-order moment of δu_1. The scaling exponents $\zeta_{u_1}(p)$ and $\zeta_{u_2}(p)$ were estimated from least-squares linear regressions over the scaling range indicated in figure 10. The resulting values are shown in figure 12 for $R_\lambda = 75$. $\zeta_{u_2}(p)$ is appreciably smaller than $\zeta_{u_1}(p)$ for all values of p. The difference between these two exponents increases with p. Also shown in figure 12 are scaling exponents obtained from K41, the lognormal (LN) model (K62) with $\mu = 0.2$ and the She–Leveque (SL) model (She & Leveque 1994). The present

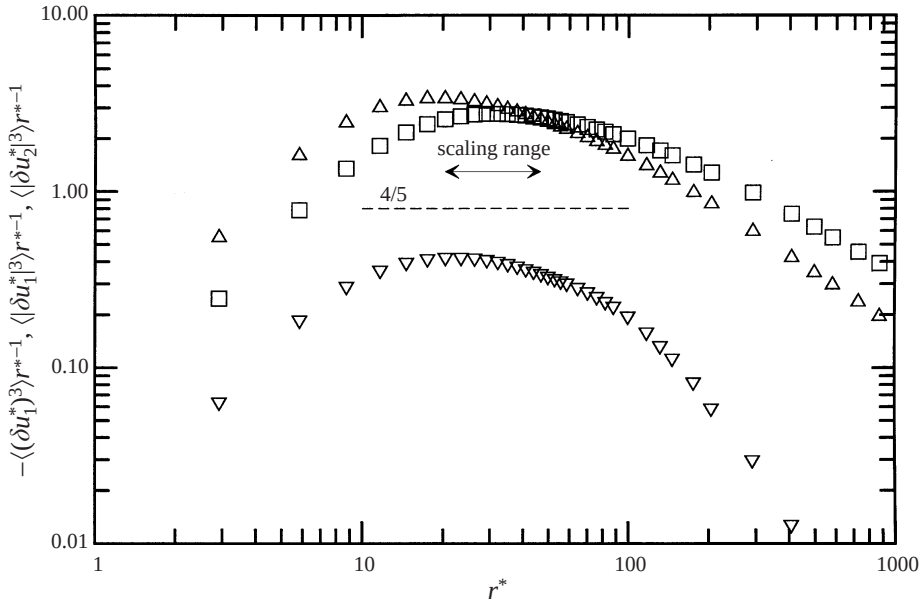

FIGURE 10. Kolmogorov-normalized third-order moment of δu_1, $|\delta u_1|$ and $|\delta u_2|$, each multiplied by r^{*-1} for the case of $R_\lambda = 75$. ∇, $-\langle(\delta u_1^*)^3\rangle r^{*-1}$; $\square$, $\langle|\delta u_1^{*3}|\rangle r^{*-1}$; $\triangle$, $\langle|\delta u_2^{*3}|\rangle r^{*-1}$; - - -, (4.2). Arrowed solid line indicates extent of the scaling range.

values of $\zeta_{u_1}(p)$ depart from K41 much more than from LN and SL. The latter two represent the present values quite satisfactorily for $p \leqslant 6$. The departure from K41 is greater for $\zeta_{u_2}(p)$ than for $\zeta_{u_1}(p)$.

The scaling exponents for transverse velocity increments can also be obtained by plotting $\langle|\delta u_2|^p\rangle$ against $\langle|\delta u_2|^3\rangle$ (e.g. Camussi & Guj 1996; Camussi *et al.* 1996; Cerutti & Meneveau 1998) over a range where $\langle|\delta u_2|^3\rangle$ varies linearly with r as shown in figure 10. The plateau in $r^{-1}\langle|\delta u_2|^3\rangle$ is even smaller than that in $r^{-1}\langle|\delta u_1|^3\rangle$. The scaling of $\langle|\delta u_2|^p\rangle$ extends to the dissipative range when it is plotted against $\langle|\delta u_2|^3\rangle$ and the curvature exhibited in figure 11(*b*) disappears. The resulting values of $\zeta_\perp(p)$ are also shown in figure 12. Note that $\zeta_\perp(p)$ is used here to differentiate it from $\zeta_{u_2}(p)$. Clearly, $\zeta_\perp(2) > \zeta_{u_1}(2)$ and $\zeta_\perp(p) < \zeta_{u_1}(p)$ for $p \geqslant 4$, consistent with the previous experimental results of Camussi & Guj (1996) and Camussi *et al.* (1996). The present (ESS) values of $\zeta_{u_1}(p)$ and $\zeta_\perp(p)$ are essentially independent of R_λ (results not shown here) within the experimental uncertainty. This result seems consistent with the DNS data of Grossmann *et al.* (1997). However, in the context of ESS, the use of $\langle|\delta u_2|^3\rangle$, as reference for $\langle|\delta u_2|^p\rangle$, seems less justified than that of $\langle|\delta u_1|^3\rangle$, since $\langle(\delta u_2)^3\rangle$ should be zero in isotropic turbulence. For this reason, we have preferred to use $\langle|\delta u_1|^3\rangle$ for estimating $\zeta_{u_2}(p)$ in the present study.

In order to account for the possibly different influences of ϵ and ω^2 on the scaling of the longitudinal and transverse velocity increments, Chen *et al.* (1997*a*) proposed a modified model which they called the refined similarity hypothesis for transverse velocity increments (RSHT). While RSH does not distinguish between δu_1 and δu_2 (or δu_3), RSHT retains RSH only for δu_1:

$$\delta u_1 \sim (r\epsilon_r)^{1/3} \tag{5.1}$$

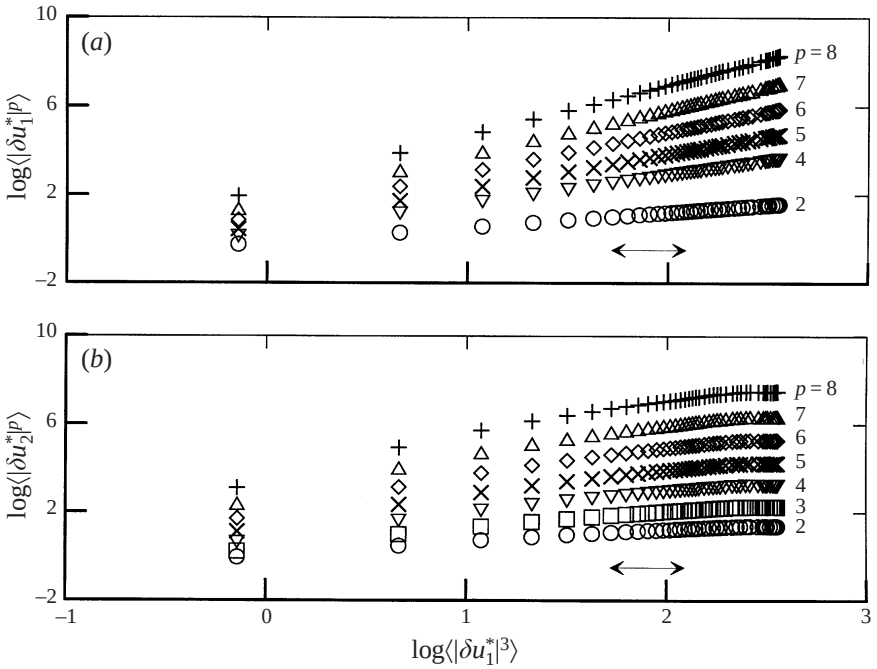

FIGURE 11. Moments of order p (2 to 8) of $\langle|\delta u_1^*|^p\rangle$ and $\langle|\delta u_2^*|^p\rangle$ as a function of $\langle|\delta u_1^*|^3\rangle$ for $R_\lambda = 75$. (*a*) $\langle|\delta u_1^*|^p\rangle$; (*b*) $\langle|\delta u_2^*|^p\rangle$. Arrowed solid horizontal lines indicate extent of the scaling range.

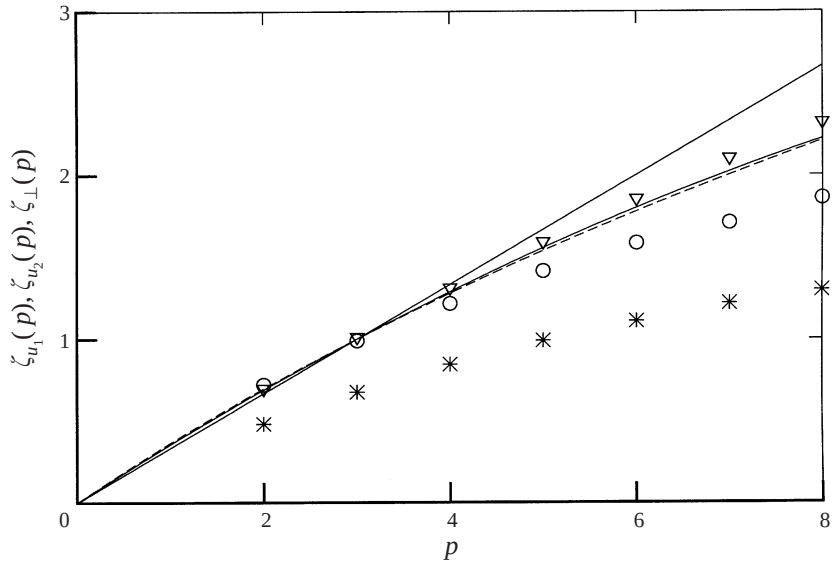

FIGURE 12. Scaling exponents for longitudinal and transverse velocity increments as a function of p for $R_\lambda = 75$. ▽, $\zeta_{u_1}(p)$; *, $\zeta_{u_2}(p)$; ○, $\zeta_\perp(p)$; —, K41; — - —, LN; – –, SL.

and proposes that δu_2 is given by

$$\delta u_2 \sim (r v \omega_r^2)^{1/3}, \tag{5.2}$$

where ϵ_r and ω_r^2 are the locally averaged values of ϵ and ω^2 respectively. Since $\langle(\delta u_1)^p\rangle$

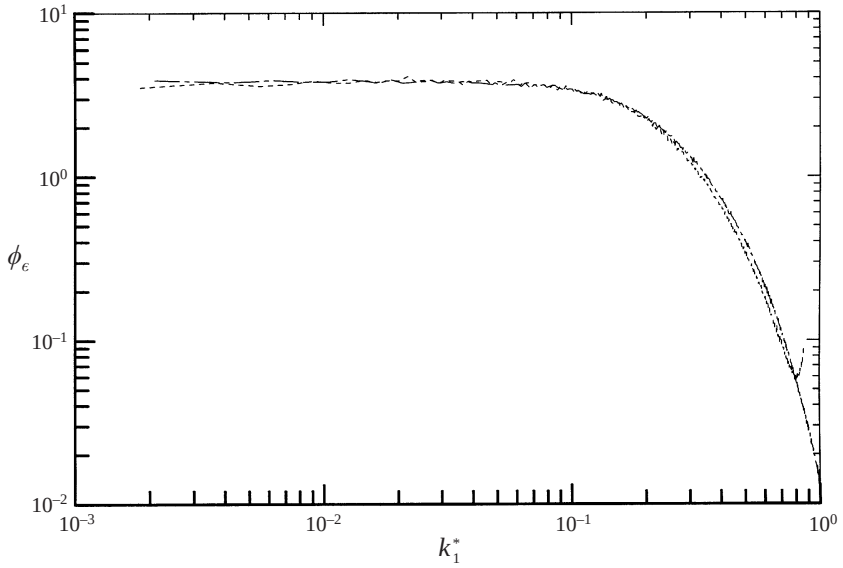

FIGURE 13. Comparison of energy dissipation rate spectra obtained with the present one-component vorticity probe (equation (5.5)) and the three-component vorticity probe described in Antonia *et al.* (1998). Present: — - —, ϕ_ϵ ($R_\lambda = 75$). Three-component vorticity probe: - - -, ϕ_{ϵ_f}.

and $\langle(\delta u_2)^p\rangle$ scale as $r^{\zeta^L(p)}$ and $r^{\zeta^T(p)}$ over the IR, it is assumed that $\langle\epsilon_r^p\rangle$ and $\langle(\omega_r^2)^p\rangle$ scale as $r^{\tau^d(p)}$ and $r^{\tau^v(p)}$ respectively. After equating the corresponding exponents of r,

$$\left.\begin{aligned}\zeta^L(p) &= p/3 + \tau^d(p/3),\\ \zeta^T(p) &= p/3 + \tau^v(p/3).\end{aligned}\right\} \tag{5.3}$$

The superscripts L and T have been introduced because $\zeta^L(p)$ and $\zeta^T(p)$ need not, in general, be the same as $\zeta_{u_1}(p)$ and $\zeta_{u_2}(p)$. The exponents $\tau^d(p/3)$ and $\tau^v(p/3)$ can be inferred from the rate of change of $\langle(\epsilon_r)^{p/3}\rangle$ and $\langle(\omega_r^2)^{p/3}\rangle$ with respect to r over the same scaling range for which $\zeta_{u_1}(p)$ and $\zeta_{u_2}(p)$ were obtained. RSHT can qualitatively account for the present difference between $\zeta_{u_1}(p)$ and $\zeta_{u_2}(p)$ provided $\tau^d(p/3)$ and $\tau^v(p/3)$ are both negative and the magnitude of $\tau^v(p/3)$ is larger than that of $\tau^d(p/3)$. RSHT was well supported by the DNS data of Chen *et al.* (1997*a*) for δu_2.

Although only four terms of ϵ were measured with the present one-component vorticity probe, it was assumed that an approximation to ϵ could be obtained via the following expression:

$$\epsilon = \nu[6u_{1,1}^2 + 3u_{1,2}^2 + 2u_{2,1}^2 + 2u_{1,2}u_{2,1}]. \tag{5.4}$$

The corresponding spectrum is given by

$$\phi_\epsilon(k_1) = \nu[6\phi_{u_{1,1}}(k_1) + 3\phi_{u_{1,2}}(k_1) + 2\phi_{u_{2,1}}(k_1) + 2Co_{1221}(k_1)], \tag{5.5}$$

where Co_{1221} is the cospectrum between $u_{1,2}$ and $u_{2,1}$ and is defined such that $\int_0^\infty Co_{1221}\,\mathrm{d}k_1 = \langle u_{1,2}u_{2,1}\rangle$. The spectrum $\phi_\epsilon(k_1)$ is compared in figure 13 with that obtained by Antonia *et al.* (1998) using the three-component vorticity probe (denoted as ϕ_{ϵ_f}; each term in the expression for ϕ_{ϵ_f} is corrected for the effect of spatial resolution; ϵ_f indicates the full dissipation rate). The integrals $\int_0^\infty \phi_{\epsilon_f}(k_1)\,\mathrm{d}k_1$ and $\int_0^\infty \phi_\epsilon(k_1)\,\mathrm{d}k_1$, which should be equal to 1, agree within 5%. More importantly, the agreement

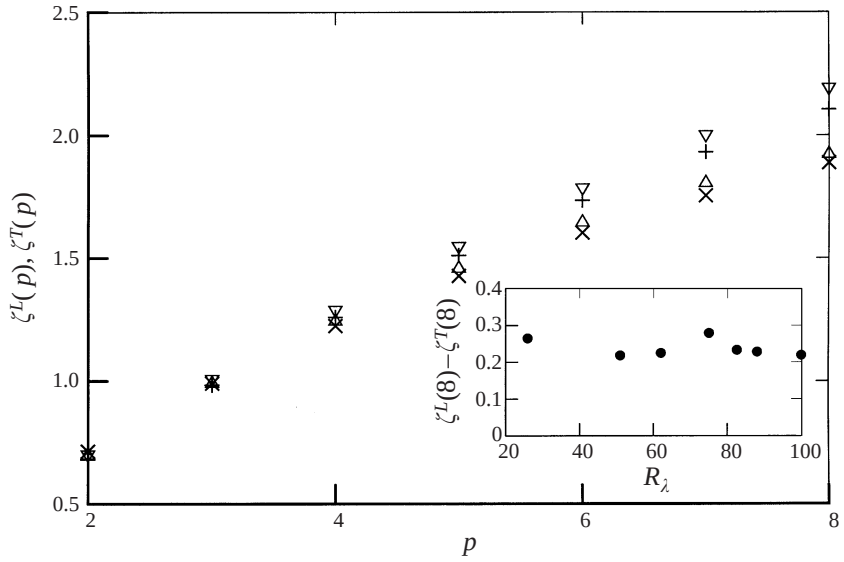

FIGURE 14. Comparison between the present values of $\zeta^L(p)$ and $\zeta^T(p)$ ($R_\lambda = 75$) and the DNS data from Chen *et al.* (1997*a*) ($R_\lambda = 216$). Present: +, $\zeta^L(p)$; ×, $\zeta^T(p)$. Chen *et al.* (1997*a*): ▽, $\zeta^L(p)$; △, $\zeta^T(p)$. The inset shows the R_λ dependence of the difference $\zeta^L(8) - \zeta^T(8)$.

between $\phi_{\epsilon_f}(k_1)$ and $\phi_\epsilon(k_1)$ is quite good in the region $0.02 \leqslant k_1^* \leqslant 0.1$, the region most relevant to scaling exponent estimations. These observations provide some justification for the use of (5.4). The exponents $\tau^d(p/3)$ and $\tau^v(p/3)$ were estimated from distributions of $\langle \epsilon_r^{p/3} \rangle$ and $\langle (\omega_3^2)_r^{p/3} \rangle$ over the scaling range. The resulting values of $\zeta^T(p)$ and $\zeta^L(p)$ are shown in figure 14. The values of $\zeta^L(p)$ and $\zeta^T(p)$ from the DNS data of Chen *et al.* (1997*a*), are also shown. There is good agreement for $\zeta^L(p)$ and $\zeta^T(p)$ between the present and the DNS data. For the present data, the different magnitudes of the inequalities $\zeta^T(p) < \zeta^L(p)$ and $\zeta_{u_2}(p) < \zeta_{u_1}(p)$ are not consistent with RSHT. It is nonetheless evident that RSHT only partially accounts for the present inequality $\zeta_{u_1}(p) < \zeta_{u_2}(p)$. It is found that for $p \leqslant 3$, $\zeta^L(p) \simeq \zeta^T(p)$, with practically no variation with R_λ. For $p > 4$, $\zeta^L(p)$ and $\zeta^T(p)$ decrease with R_λ but the magnitude $[\zeta^L(p) - \zeta^T(p)]$ is essentially constant (as shown in the inset of figure 14). The present data corroborate Chen *et al.*'s (1997*b*) observations that enstrophy is more intermittent than the energy dissipation rate. The R_λ dependence of the quantities $\langle (\omega_3^2)_r^2 \rangle / \langle (\omega_3^2)_r \rangle^2$ and $\langle \epsilon_r^2 \rangle / \langle \epsilon_r \rangle^2$ is shown in figure 15 for $r^* = \lambda^*$. The former value is always larger than the latter, indicating that ω_r^2 is more intermittent than ϵ_r.

A more likely source for the inequality $\zeta_{u_1}(p) < \zeta_{u_2}(p)$ is the anisotropy in the scaling range, as discussed in the previous section in the context of $\langle (\delta u_1)^3 \rangle$ and $\langle (\delta u_1)^2 \rangle$. As R_λ increases, the ESS estimation of $\zeta_{u_1}(p)$ is nearly constant whereas $\zeta_{u_2}(p)$ increases due to the improved isotropy in the scaling range. The difference between $\zeta_{u_1}(p)$ and $\zeta_{u_2}(p)$ is consequently reduced. This asymptotic trend seems to corroborate the argument by He *et al.* (1998) that the difference between longitudinal and transverse scaling exponents may disappear in the limit of infinite R_λ. We recall here that when isotropy is satisfied in the IR, (3.1) predicts the same power-law scaling for $\phi_{u_2}(k_1)$ and $\phi_{u_1}(k_1)$; for this 'asymptotic' case, $\zeta_{u_1}(2)$ and $\zeta_{u_2}(2)$ should be identical.

The values of $\Delta\zeta(p)$ $[\equiv \zeta_{u_1}(p) - \zeta_{u_2}(p)]$ are plotted against R_λ in figure 16. Also included are the homogeneous isotropic turbulence DNS data of Chen *et al.* (1997*a*)

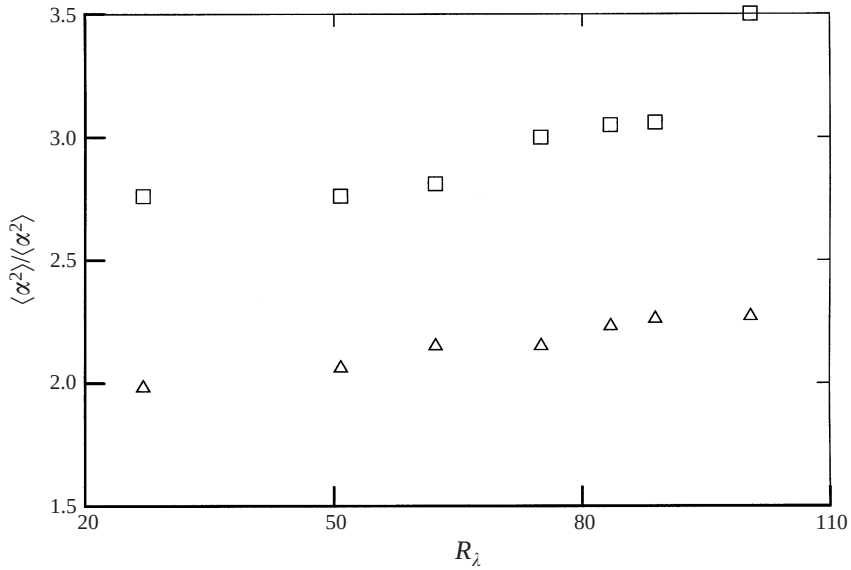

FIGURE 15. R_λ dependence of $\langle\alpha^2\rangle/\langle\alpha\rangle^2$ for the separation of r^* ($\equiv \lambda^*$). △, $\alpha = \epsilon_r$; □, $\alpha = (\omega_3^2)_r$.

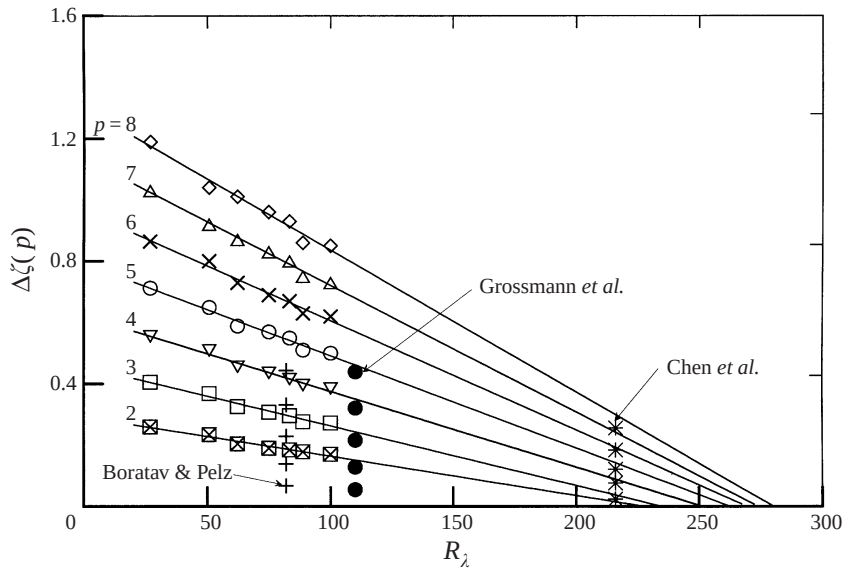

FIGURE 16. R_λ dependence of the present $\Delta\zeta(p)$ and comparison with DNS data of Chen *et al.* (1997*a*) (*, $R_\lambda = 216$, $p = 4 - 8$), Boratav & Pelz (1997) (+, $R_\lambda = 82$, $p = 4 - 8$) and Grossmann *et al.* (1997) (●, $R_\lambda = 110$, $p = 4 - 8$). The solid lines represent least-squares linear regressions to the present data for different orders.

($R_\lambda = 216$) and Boratav & Pelz (1997) ($R_\lambda = 82$) and Grossmann *et al.* (1997) ($R_\lambda = 110$). Least-squares linear regressions to the present data suggest, after extrapolation to zero, that $\Delta\zeta(p)$ should disappear at a sufficiently high value, R_λ^* say, of R_λ. The magnitude of R_λ^* increases with p. For $p = 8$, $R_\lambda^* = 280$ while for $p = 2$, $R_\lambda^* = 230$. The values of $\Delta\zeta(p)$ (for $p \geqslant 4$) estimated from the data of Chen *et al.* (1997*a*) seem consistent with these linear regressions. By contrast, $\Delta\zeta(p)$ (for

$p \geqslant 4$) inferred from ESS values of $\zeta_{u_1}(p)$ and $\zeta_{u_2}(p)$ reported by Boratav & Pelz and Grossmann *et al.* are significantly smaller than the present values, possibly because of the improved level of isotropy achieved in their simulations. For example, Boratav & Pelz used an unforced flow with a high symmetry initial condition; C_3 is about 0.8 even though R_λ is only 82. The values of $\Delta\zeta(p)$ inferred from the DNS data of Grossmann *et al.* for forced stationary turbulence ($R_\lambda = 110$), agree quite well with those of Boratav & Pelz (1997), also reflecting the good isotropy (deviations between $\langle u_1^2 \rangle$, $\langle u_2^2 \rangle$ and $\langle u_3^2 \rangle$ are less than 5%) in their simulation. It needs to be stressed that there is no real basis for a linear extrapolation in figure 16; an asymptotic approach towards R_λ^* is quite likely, in which case our values of R_λ^* should be grossly underestimated. Speculatively, even higher values of R_λ may be needed if a mean shear is present. The R_λ independence of ζ_{u_1} mentioned previously is to a significant extent an artefact of ESS. Since $\langle (\delta u_1)^n \rangle$ is cross-plotted against $\langle |\delta u_1|^3 \rangle$, it is worth keeping in mind that ESS only yields estimates of exponents relative to $\langle |\delta u_1|^3 \rangle$. When (4.6) is used, $\zeta_{u_1}(2)$, like $\zeta_{u_2}(2)$, increases with R_λ, although the difference $[\zeta_{u_1}(2) - \zeta_{u_2}(2)]$ decreases with R_λ as reported in figure 16. The variation of $\zeta_{u_1}(2)$ and $\zeta_{u_2}(2)$ with R_λ suggests that the effect of R_λ is not just confined to the magnitude of the structure functions, as shown in figures 7 and 9. It also affects the scaling of these quantities.

The intermittency parameter μ plays an important role in the theoretical framework of turbulence. Previous estimates of μ were in the range 0.2 to 0.7 (e.g. Van Atta & Yeh 1975; Nelkin 1981; Antonia, Phan-Thien & Satyaprakash 1981; Anselmet *et al.* 1984; Meneveau & Sreenivasan 1991; Praskovsky & Oncley 1994*a*, *b*; Shafi, Zhu & Antonia 1996). Sreenivasan & Kailasnath (1993) noted that this scatter is most likely due to the different definitions of μ used in various experiments. One estimate of μ is provided by the autocorrelation of ϵ (e.g. Novikov 1971; Monin & Yaglom 1975)

$$\rho_{(\epsilon)} = \frac{\langle \epsilon(x+r)\epsilon(x) \rangle}{\langle \epsilon \rangle^2} \sim r^{-\mu}, \tag{5.6}$$

when r is in the IR. With a few exceptions, the majority of the experimental estimations of ϵ to date have been based on the tenuous assumption that $\epsilon_{iso} \equiv 15\nu u_{1,1}^2$. However, the adequacy of ϵ_{iso} as a suitable surrogate for ϵ has been questioned (e.g. Gibson & Masiello 1972; Hosokawa, Oide & Yamamoto 1996; Antonia *et al.* 1998). In the present work, several possible surrogates for ϵ have been used in conjunction with (5.6). The values of μ estimated over the same scaling range as for the structure functions are shown in figure 17. All choices of ϵ yield approximately the same value of μ ($\simeq 0.1 \pm 0.03$), which is much smaller than the generally accepted value of 0.2 (e.g. Sreenivasan & Kailasnath 1993; Praskovsky & Oncley 1994*a*, *b*) at higher Reynolds numbers, also using (5.6). This discrepancy may reflect the small present values of R_λ. Note that the value of μ inferred from ϵ_f, also shown in figure 17, agrees well with that obtained from $\langle \epsilon \rangle_{iso}$.

Mydlarsky & Warhaft (1996) used $15\nu u_{1,1}^2$ and $7.5\nu u_{2,1}^2$ to estimate the value of μ from (5.6). They found that $\mu = 0$ for $R_\lambda < 100$, while for $R_\lambda > 100$, μ increases with R_λ. At $R_\lambda = 731$, $\mu \simeq 0.14$. The scaling ranges defined in figure 3 of Mydlarski & Warhaft (1996) are not the same as those indicated by the third-order longitudinal velocity structure functions shown in figure 19 of their paper. If the scaling ranges in the latter figure were used, the values of μ based on $\epsilon = 15\nu u_{1,1}^2$ would increase to 0.1 ($R_\lambda = 99$) and 0.15 ($R_\lambda = 377$). For their simulation ($R_\lambda = 110$), Vincent & Meneguzzi (1991), also using (5.6), obtained values of μ comparable to ours. Referring to Kraichnan (1974), they argued that μ, as it appears in (5.6), is not a pure IR quantity even

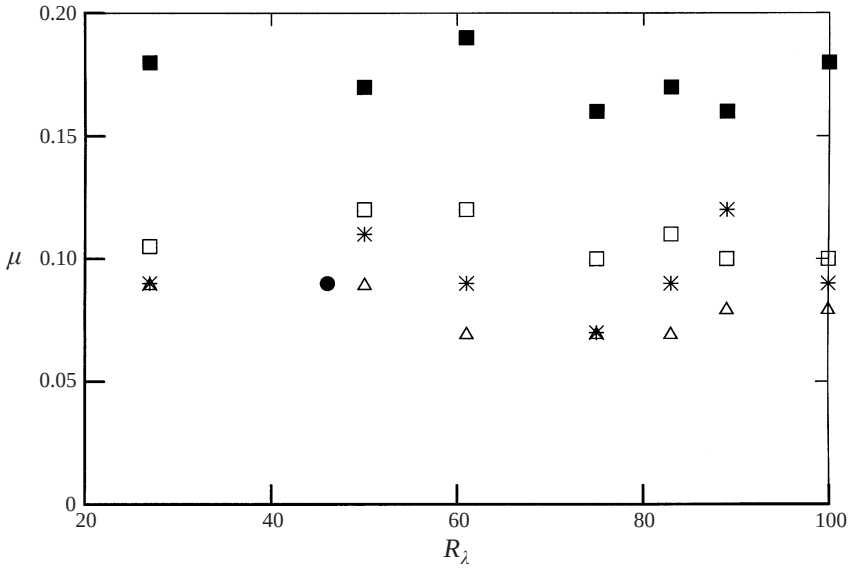

FIGURE 17. Estimates of μ using different expressions for ϵ and compared with those obtained from $\zeta_{u_1}(6)$. △, $\epsilon \sim \langle u_{1,1}^2 \rangle$; *, $\epsilon \sim \langle \omega_3^2 \rangle$; □, $\epsilon \sim$ equation (5.4); ●, ϵ_f (from the three-component vorticity probe of Antonia *et al.* 1998); ■, from the sixth-order velocity structure function, i.e. $\langle (\delta u_1)^6 \rangle \sim r^{\zeta_{u_1}(6)}$ ($\zeta_{u_1}(6) = 2 - \mu$).

when r is in the IR. μ should therefore contain some influence from the DR scales, especially when R_λ is small (see also Sreenivasan & Antonia 1997; Grossmann *et al.* 1997). As R_λ increases, the influence from the DR should diminish and μ, obtained from (5.6), should increase approaching the value of about 0.2 at sufficiently large R_λ. Measurements in high-R_λ flows show that μ obtained from (5.6) is approximately constant ($\simeq$ 0.2–0.25) (e.g. Chambers & Antonia 1984; Sreenivasan & Kailasnath 1993; Praskovsky & Oncley 1994*a*, *b*). However, the intermittency exponent μ in (5.6) is ill-defined, as noted by Praskovsky & Oncley (1994*b*) and L'vov & Procaccia (1995). These authors argued that no power-law behaviour in the IR can be expected from this definition at finite values of R_λ. So (5.6) can only be considered as reasonably approximate within the IR.

The sixth-order velocity structure function provides another measure of μ since $\langle (\delta u_1)^6 \rangle \sim r^{2-\mu}$ (i.e. $\mu = 2 - \zeta_{u_1}(6)$) in the IR. The average value of μ estimated in this manner is about 0.17 ± 0.05. This value is nearly independent of R_λ if $\zeta_{u_1}(6)$ is estimated using ESS and is closer to the 'consensus' value of 0.2 (e.g. Antonia *et al.* 1982; Anselmet *et al.* 1984; Sreenivasan & Kailasnath 1993).

6. R_λ dependence of the fourth-order velocity derivative correlations

Distributions of the ratios A ($\equiv I_2/I_1$), B ($\equiv I_3/I_1$) and C ($\equiv I_4/I_1$) are shown in figure 18. Also shown in this figure are values of A, B and C inferred from isotropic DNS data (Siggia 1981, R_λ = 60–90; Kerr 1985, R_λ = 9–83) and the grid turbulence data of Tsinober *et al.* (1992). Values of A and C from the three-component vorticity probe are also shown (I_3 was not available in this latter experiment). There is satisfactory agreement between values of A (figure 18*a*) obtained from different methods, except for the values of Siggia which are about 30% higher than the

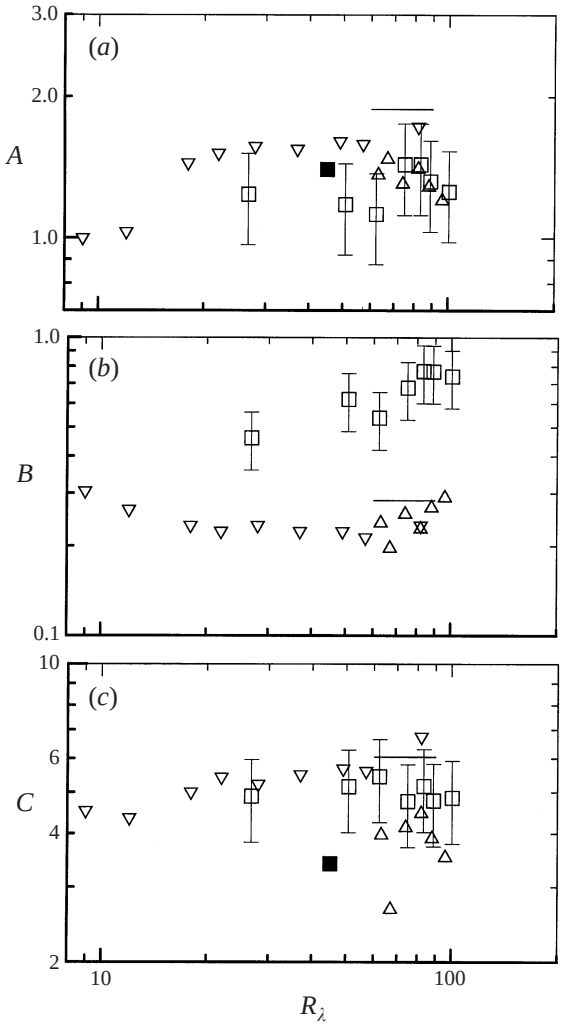

FIGURE 18. R_λ dependence of invariants defined by Siggia (1981). (*a*) A ($\approx I_2/I_1$); (*b*) B ($\approx I_3/I_1$); (*c*) C ($\approx I_4/I_1$). □, Present; ▽, Kerr (1985); ■, three-component vorticity measurement; △, Tsinober *et al.* (1992); —, Siggia (1981). Error bars indicate experimental uncertainties for the present data.

others. The data of Kerr (1985) suggest that A increases weakly with R_λ ($\sim R_\lambda^{0.11}$) whereas the present values and those of Tsinober *et al.* show no discernible R_λ dependence, indicating that the present measured values of I_2 reveal the same power-law dependence on R_λ as I_1. There is a large scatter in B (figure 18*b*): the present data have much larger magnitudes than those of Siggia, Kerr and Tsinober *et al.* Unlike the present and Tsinober *et al.*'s (1992) values of C (figure 18*c*) which show practically no R_λ dependence, Kerr's data indicate a $R_\lambda^{0.19}$ dependence. The value of C from the three-component vorticity probe is 30% smaller than for the present measurement. This may be due to the poor spatial resolution of the probe at this location ($\Delta x_2^* \simeq \Delta x_3^* \simeq 6$). This probe was also used in a turbulent far wake ($R_\lambda = 40$), with $\Delta x_2^* \simeq \Delta x_3^* = 3.5$; the resulting value of C was about 5.2.

The four rotational invariants defined in (1.1) can also be normalized as follows

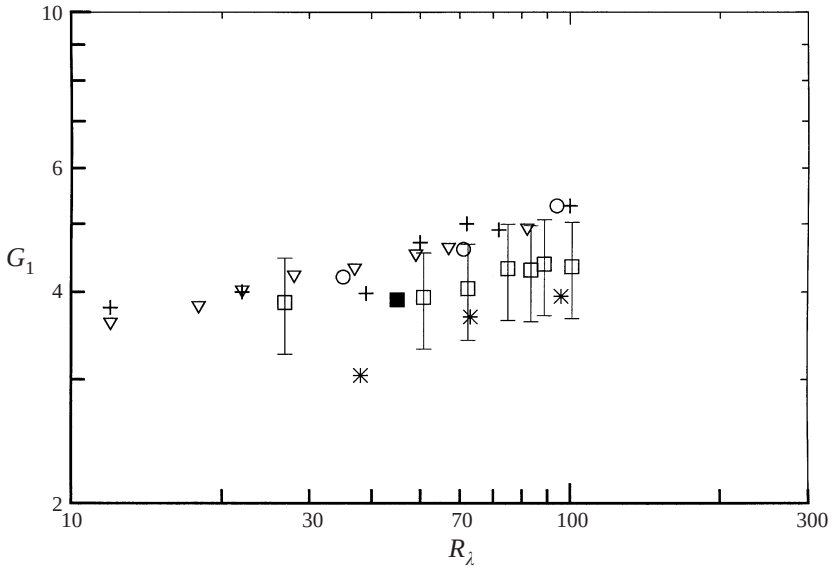

FIGURE 19. Power-law dependence of G_1 on R_λ ($\sim R_\lambda^\alpha$) and comparison with other data. □, Present ($\alpha = 0.17 \pm 0.03$); ▽, Kerr (1985) (0.18 ± 0.02); +, Kuo & Corrsin (1971) (0.2 ± 0.05); ○, Jimenez *et al.* (1993) (0.25 ± 0.02); *, Gotoh & Rogallo (1994) (0.21 ± 0.04); ■, three-component vorticity probe. Error bars indicate experimental uncertainties for the present data.

(Kerr 1985):

$$G_1 = \frac{15}{7}\,\frac{I_1}{\langle e^2\rangle^2}, \quad G_2 = 3\frac{I_2}{\langle\omega^2\rangle\langle e^2\rangle}, \quad G_3 = 3\frac{I_3}{\langle\omega^2\rangle\langle e^2\rangle}, \quad G_4 = \frac{9}{5}\,\frac{I_4}{\langle\omega^2\rangle^2}. \tag{6.1}$$

The corresponding Gaussian values for G_i are 3 ($i = 1$), 3 ($i = 2$), 1 ($i = 3$) and 3 ($i = 4$). G_1 and G_4 can be identified with the flatness factors of $u_{1,1}$ and ω_i ($i = 1, 2, 3$) respectively if isotropy is assumed. The implication of Kolmogorov (1941) is that the limiting values of the flatness factors of velocity derivatives should be independent of the large-scale properties of the turbulence and should reach universal constant values at large enough R_λ. The R_λ dependences of G_i ($i = 1$–4) are shown in figures 19–21. All the values of G_1 or $F_{u_{1,1}}$ shown in figure 19 are larger than the Gaussian value of 3. There is good agreement between the experimental values of Kuo & Corrsin (1971) and the numerical values of Kerr (1985) and Jimenez *et al.* (1993). The DNS values of Gotoh & Rogallo (1994) are quite small. Kuo & Corrsin (1971) found that the flatness factor $F_{u_{1,1}} \sim R_\lambda^{0.2}$ for $R_\lambda < 200$, and, following a transition zone up to $R_\lambda \simeq 500$, $F_{u_{1,1}}$ increases more rapidly with R_λ. The present values of G_1 agree well with those obtained from the three-component vorticity probe. A power-law fit to the present data in figure 19 yielded an exponent of 0.17 ± 0.03, which is close to the value obtained by Kuo & Corrsin (1971) and Kerr (1985) (0.18 ± 0.03).

The present distributions of G_2 and G_3 are compared with those of Kerr (1985) and Tsinober *et al.* in figure 20. For values of G_2 (figure 20*a*), which are larger than the Gaussian value of 3 except for Kerr's simulation at small R_λ, there is good agreement between the present and Tsinober *et al.*'s data. These values are typically about 10% smaller than Kerr's values at a comparable R_λ. Kerr's data for G_2 indicate a R_λ dependence with an exponent α of 0.29 ($\pm$0.03), which is comparable to the present value of 0.22 ($\pm$0.05). Unlike Kerr's and Tsinober *et al.*'s values of G_3, which

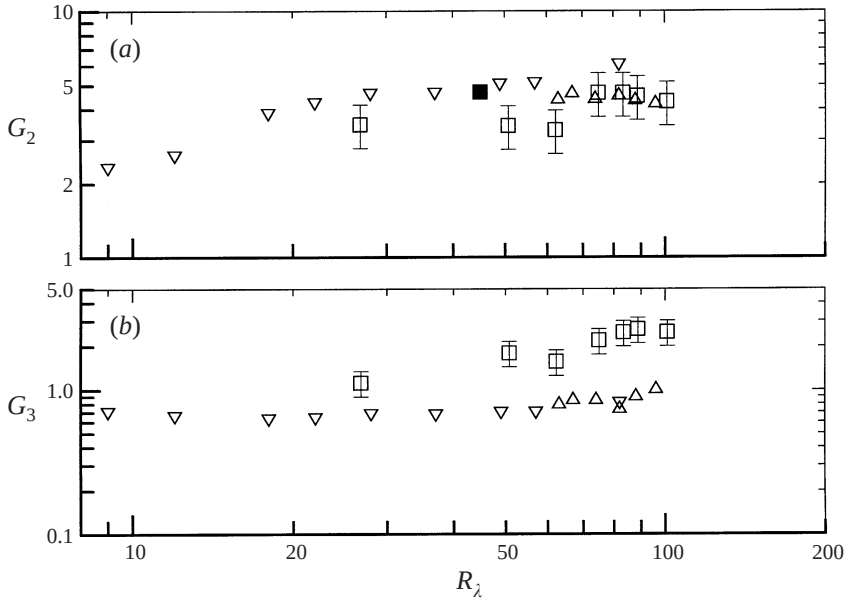

FIGURE 20. Power-law dependence of G_2 and G_3 on R_λ ($\sim R_\lambda^\alpha$) and comparison with other data. (*a*) G_2: □, Present ($\alpha = 0.22 \pm 0.05$); ▽, Kerr (1985) ($\alpha = 0.29 \pm 0.03$); △, Tsinober *et al.* (1992); ■, three-component vorticity probe. (*b*) G_3: □, Present ($\alpha = 0.66 \pm 0.09$); ▽, Kerr (1985) ($\alpha = 0.16 \pm 0.04$); △, Tsinober *et al.* (1992). Error bars indicate experimental uncertainties for the present data.

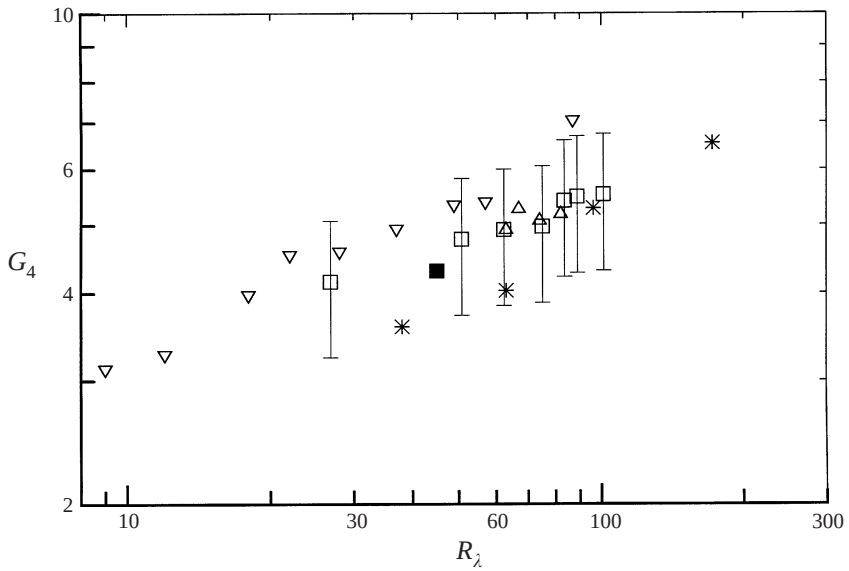

FIGURE 21. Power-law dependence of G_4 on R_λ ($\sim R_\lambda^\alpha$) and comparison with other data. □, Present ($\alpha = 0.24 \pm 0.02$); ▽, Kerr (1985) (0.37 ± 0.05); *, Gotoh & Rogallo (1994) (0.42 ± 0.03); △, Tsinober *et al.* (1992); ■, three-component vorticity probe. Error bars indicate experimental uncertainties for the present data.

are smaller than the Gaussian value ($\equiv 1$), the present values of G_3 (figure 20*b*) are significantly larger than 1. Kerr and Tsinober *et al.* argued that the small values of G_3 imply some alignment in the small-scale turbulent structures. All the values of G_3 increase monotonically with R_λ for $R_\lambda \geqslant 20$; the present power-law exponent for G_3 (0.66 ± 0.09) is about four times larger than that of Kerr (0.16 ± 0.04). The large difference for G_3 between Kerr, Tsinober *et al.* and the present measurement needs to be resolved, although it may simply reflect the large experimental uncertainty in estimating G_3.

Figure 21 compares the present values of G_4 with those of Tsinober *et al.*, Kerr (1985) and Gotoh & Rogallo (1994). The Tsinober *et al.* data agree well with the present data for $x_1/M \geqslant 37$. The values of G_4 from the three-component vorticity measurement are about 10% smaller than the present values. From power-law fits in the range $R_\lambda \geqslant 30$, we find exponents of 0.24 ± 0.05, 0.37 ± 0.03 and 0.42 ± 0.03 for our data, Kerr and Gotoh & Rogallo respectively. Compared with figure 19, the exponents in figure 21 for G_4 are higher. As suggested by Kerr (1985), different power-law exponents may be needed for the rate of strain and the vorticity. The Gotoh & Rogallo data seem to support this suggestion more clearly. The present data, on the other hand, indicate that the exponent for G_4 ($= 0.24 \pm 0.05$) is only marginally bigger than that for G_1 ($= 0.17 \pm 0.03$); this difference may not be significant in view of the experimental uncertainty.

7. Conclusions

The transverse component ω_3 of the fluctuating vorticity vector was measured in grid turbulence for values of the Taylor microscale Reynolds number R_λ in the range 27–100. Local isotropy of the small-scale structures was examined extensively. In particular, the measured spectra of u_2 and ω_3 were compared with those calculated using isotropic relations. The wavenumber range over which local isotropy is satisfied by $\phi^*_{u_2}(k_1^*)$ extends to lower values of k_1^* as R_λ increases. By contrast, $\phi^*_{\omega_3}(k_1^*)$ shows quite good agreement ($\pm 10\%$) with isotropy at nearly all wavenumbers, supporting the conclusion by Antonia & Kim (1994) that the vorticity spectra tend to satisfy isotropy almost independently of R_λ.

The inequality between scaling exponents, estimated with a modified ESS method, for the longitudinal and transverse velocity increments can only partially be attributed to a difference in intermittency between the locally averaged energy dissipation rate and the enstrophy. The difference $[\zeta^L(p) - \zeta^T(p)]$ inferred, using RSH and RSHT, from the scaling range behaviours of $\langle \epsilon_r^{p/3} \rangle$ and $\langle (\omega_3^2)_r^{p/3} \rangle$ is much smaller than the difference $[\zeta_{u_1}(p) - \zeta_{u_2}(p)]$, which was directly obtained from the longitudinal and transverse velocity increments. Although the former difference agrees quite well with the difference $[\zeta_{u_1}(p) - \zeta_\perp(p)]$, where $\zeta_\perp(p)$ is obtained by plotting $\langle |\delta u_2|^p \rangle$ against $\langle |\delta u_2|^3 \rangle$, this agreement may be fortuitous since there is no theoretical basis for $\langle |\delta u_2|^3 \rangle$. A more likely source of the inequality $\zeta_{u_2}(p) < \zeta_{u_1}(p)$ is the scaling-range anisotropy associated with the present small values of R_λ. The second- and third-order moments of δu_1 (§ 4) clearly indicate that the anisotropy decreases with increasing R_λ. It would therefore be reasonable to expect the difference $[\zeta_{u_1}(p) - \zeta_{u_2}(p)]$ to decrease as R_λ increases. The present R_λ dependence of $[\zeta_{u_1}(p) - \zeta_{u_2}(p)]$ strongly supports this expectation. In particular, the inequality $\zeta_{u_2}(2) < \zeta_{u_1}(2)$ should disappear when $R_\lambda \simeq 1000$. Speculatively, a value of R_λ of order 10^4 may be needed if a mean shear is present.

The four invariants I_α ($\alpha = 1$ to 4) proposed by Siggia (1981) were determined from the data obtained with the transverse vorticity probe. For any particular value of α, the

magnitude of I_α/I_1 is, to a first approximation, nearly constant over the present range of R_λ, implying that all the I_α are interdependent. Consequently, all fourth-order velocity derivative correlations should be proportional to $\langle u_{1,1}^4 \rangle$ in isotropic turbulence. This appears to be approximately satisfied by the present data. Correspondingly, different fourth-order velocity derivative correlations increase with R_λ at approximately the same rate allowing for the experimental uncertainty. This contrasts with the suggestions by Kerr (1985) and Gotoh & Rogallo (1994) – based on DNS isotropic turbulence data over a R_λ range comparable to that of the present experiment – that at least two power-law exponents are needed, one for the rate of strain and the other for vorticity. It is however consistent with our earlier conclusion that the statistical differences between ϵ_r and $(\omega_3^2)_r$ only marginally account for the difference of $[\zeta_{u_1}(p) - \zeta_{u_2}(p)]$.

The support of the Australian Research Council is gratefully acknowledged. R.A.A. would like to thank M. Nelkin and N. Phan-Thien for several interesting discussions in connection with the fourth-order rotational invariants. We especially acknowledge our continuing collaboration with F. Anselmet and L. Danaila at the IRPHE. We also thank L. Mydlarski for making the second- and third-order structure functions at $R_\lambda = 671$ available to us.

REFERENCES

Anselmet, F., Gagne, Y., Hopfinger, E. J. & Antonia, R. A. 1984 Higher-order velocity structure functions in turbulent shear flows. *J. Fluid Mech.* **140**, 63–89.

Antonia, R. A. & Kim, J. 1994 A numerical study of local isotropy of turbulence. *Phys. Fluids* A **6**, 834–841.

Antonia, R. A., Phan-Thien, N. & Satyaprakash, B. R. 1981 Autocorrelation and spectrum of dissipation fluctuations in a turbulent jet. *Phys. Fluids* **24**, 554–555.

Antonia, R. A., Satyaprakash, B. R. & Hussain, A. K. M. F. 1982 Statistics of fine scale velocity in turbulent plane and circular jet. *J. Fluid Mech.* **119**, 55–89.

Antonia, R. A., Zhou, T. & Zhu, Y. 1998 Three-component vorticity measurements in a turbulent grid flow. *J. Fluid Mech.* **374**, 29–57.

Antonia, R. A., Zhu, Y. & Kim, J. 1993 On the measurement of lateral velocity derivatives in turbulent flows. *Exps. Fluids* **15**, 65–69.

Antonia, R. A., Zhu, Y. & Shafi, H. S. 1996 Lateral vorticity measurements in a turbulent wake. *J. Fluid Mech.* **323**, 173–200.

Batchelor, G. K. 1951 Pressure fluctuations in isotropic turbulence. *Proc. Camb. Phil. Soc.* **47**, 359–374.

Batchelor, G. K. & Townsend, A. A. 1947 Decay of vorticity in isotropic turbulence. *Proc. R. Soc. Lond.* A **190**, 534–550.

Benzi, R., Ciliberto, S., Tripiccione, R., Baudet, C., Massaioli, F. & Succi, S. 1993 Extended self-similarity in turbulent flows. *Phys. Rev.* E **48**, R29–32.

Boratav, O. N. & Pelz, R. B. 1997 Structures and structure functions in the inertial range of turbulence. *Phys. Fluids* **9**, 1400–1415.

Browne, L. W. B., Antonia, R. A. & Chua, L. P. 1989 Calibration of X-probe for turbulent flow measurement. *Exps. Fluids* **7**, 201–208.

Camussi, R., Barbagallo, D., Guj, G. & Stella, F. 1996 Transverse and longitudinal scaling laws in non-homogeneous low *Re* turbulence. *Phys. Fluids* **8**, 1181–1191.

Camussi, R. & Benzi, R. 1997 Hierarchy of transverse structure functions. *Phys. Fluids* **9**, 257–259.

Camussi, R. & Guj, G. 1996 Experimental analysis of scaling laws in low and moderate Re_λ in grid-generated turbulence. *Exps. Fluids* **20**, 199–209.

Cerutti, S. R. & Meneveau, C. 1998 Intermittency and relative scaling of subgrid-scale energy dissipation in isotropic turbulence. *Phys. Fluids* **10**, 928–937.

Chambers, A. J. & Antonia, R. A. 1984 Atmospheric estimates of power-law exponents μ and μ_θ. *Boundary-Layer Met.* **28**, 343–352.

Chen, S., Sreenivasan, K. R. & Nelkin, M. 1997*a* Inertial range scalings of dissipation and enstrophy in isotropic turbulence. *Phys. Rev. Lett.* **79**, 1253–1256.

Chen, S., Sreenivasan, K. R., Nelkin, M. & Cao, N. 1997*b* A refined similarity hypothesis for transverse structure functions. *Phys. Rev. Lett.* **79**, 1253.

Danaila, L., Anselmet, F., Zhou, T. & Antonia, R. A. 1999 A generalization of Yaglom's equation which accounts for the large-scale forcing in heated grid turbulence. *J. Fluid Mech.* **391**, 359–372.

Dhruva, B., Tsuji, Y. & Sreenivasan, K. R. 1997 Transverse structure functions in high-Reynolds-number turbulence. *Phys. Rev.* E **56**, R4928–R4930.

Gibson, C. H. & Masiello, P. J. 1972 Observations of the variability of dissipation rates of turbulent velocity and temperature fields. In *Statistical Models and Turbulence* (ed. M. Rosenblatt & C. W. Van Atta), pp. 427–453. Springer.

Gotoh, T. & Rogallo, R. S. 1994 Statistics of pressure and pressure gradient in homogeneous isotropic turbulence. *Proc. of the Summer Program, Center for Turbulence Research*, pp. 189–205.

Grossmann, S., Lohse, D. & Reeh, A. 1997 Different intermittency for longitudinal and transversal turbulent fluctuations. *Phys. Fluids* **9**, 3817–3825.

He, G., Chen, S., Kraichnan, R. H., Zhang, R. & Zhou, Y. 1998 Statistics of dissipationand enstrophy induced by localized vortices. *Phys. Rev. Lett.* **81**, 4636–4639.

Herweijer, J. A. & Water, W. van de 1995 Transverse structure functions of turbulence. In *Advances in Turbulence V* (ed. R. Benzi), pp. 210–216. Kluwer.

Hirota, M., Fujita, H. & Yokosawa, H. 1988 Influences of velocity gradient on hot-wire anemometry with an X-wire probe. *J. Phys.* E: *Sci. Instrum.* **21**, 1077–1084.

Hosokawa, I., Oide, S. & Yamamoto, K. 1996 Isotropic turbulence: important differences between true dissipation rate and its one-dimensional surrogate. *Phys. Rev. Lett.* **77**, 4548–4551.

Jimenez, J., Wray, A. A., Saffman, P. G. & Rogallo, R. S. 1993 The structure of intense vorticity in isotropic turbulence. *J. Fluid Mech.* **255**, 65–90.

Kahalerras, H., Malecot, Y. & Gagne, Y. 1996 Transverse velocity structure functions in developed turbulence. In *Advances in Turbulence VI* (ed. S. Gavrilakis, L. Machiels & P. A. Monkewitz), pp. 235–238. Kluwer.

Kármán, T. Von & Howarth, L. 1938 On the statistical theory of isotropic turbulence. *Proc. R. Soc. Lond.* A **164**, 192–215.

Kawall, J. G., Shokr, M. & Keffer, J. F. 1983 A digital technique of the simultaneous measurement of streamwise and lateral velocities in turbulent flows. *J. Fluid Mech.* **133**, 83–112.

Kerr, R. M. 1985 Higher-order derivative correlations and the alignment of small-scale structures in isotropic numerical turbulence. *J. Fluid Mech.* **153**, 31–58.

Kim, J. & Antonia, R. A. 1993 Isotropy of small scales of turbulence at low Reynolds number. *J. Fluid Mech.* **251**, 219–238.

Kistler, A. L. & Vrebalovich, T. 1966 Grid turbulence at large Reynolds numbers. *J. Fluid Mech.* **26**, 37–47.

Kolmogorov, A. N. 1941 The local structure of turbulence in an incompressible viscous fluid for very large Reynolds numbers. *Dokl. Akad. Nauk. SSSR* **30**, 301–305.

Kolmogorov, A. N. 1962 A refinement of previous hypothesis concerning the local structure of turbulence in a viscous incompressible fluid at high Reynolds number. *J. Fluid Mech.* **13**, 82–85.

Kraichnan, R. H. 1974 On Kolmogorov's inertial range theories. *J. Fluid Mech.* **62**, 305–330.

Kuo, A. K. & Corrsin, S. 1971 Experiments on internal intermittency and fine-structure distribution functions in fully turbulent fluid. *J. Fluid Mech.* **50**, 285–319.

Lindborg, E. 1999 Correction to four-fifths law due to variations of the dissipation. *Phys. Fluids* **11**, 510–512.

Lohse, D. & Müller-Gvroeling, A. 1995 Bottleneck effects in turbulence: scaling phenomena in r versus p space. *Phys. Rev. Lett.* **74**, 1747–1750.

L'vov, V. S. & Procaccia, I. 1995 Correlations of velocity differences and energy dissipation as an element in the subcritical scenario for non-Kolmogorov scaling in turbulence. *Europhys. Lett.* **29**, 291–296.

L'vov, V. S. & Procaccia, I. 1996 The universal scaling of exponents of anisotropy in turbulence and their measurement. *Phys. Fluids* **8**, 2565–2567.

MENEVEAU, C. & SREENIVASAN, K. R. 1991 The multifractal nature of turbulent energy dissipation, *J. Fluid Mech.* **224**, 429–484.

MOFFAT, R. J. 1988 Describing the uncertainties in experimental results. *Exptl Thermal Fluid Sci.* **1**, 3–17.

MOHAMED, M. S. & LARUE, J. C. 1990 The decay power law in grid-generated turbulence. *J. Fluid Mech.* **219**, 195–214.

MONIN, A. S. & YAGLOM, A. M. 1975 *Statistical Fluid Mechanics*, vol. 2. MIT Press.

MYDLARSKI, L. & WARHAFT, Z. 1996 On the onset of high-Reynolds number grid-generated wind tunnel turbulence. *J. Fluid Mech.* **320**, 331–368.

NELKIN, M. 1981 Do the dissipation fluctuations in high Reynolds number turbulence define a universal exponent? *Phys. Fluids* **24**, 556–558.

NELKIN, M. 1999 Enstrophy and dissipation must have the same scaling exponent in the high Reynolds number limit of fluid turbulence. *Phys. Fluids* **11**, 2202–2204.

NOULLEZ, A., WALLACE, G., LEMPERT, W., MILES, R. B. & FRISCH, U. 1997 Transverse velocity increments in turbulent flow using the RELIEF technique. *J. Fluid Mech.* **339**, 287–307.

NOVIKOV, E. A. 1971 Intermittency and scale similarity in the structure of a turbulent flow. *Appl. Math. Mech.* **35**, 231–241.

PARK, S. R. & WALLACE, J. M. 1993 The influence of instantaneous velocity gradients on turbulence properties measured with multi-sensor hot-wire probes. *Exps. Fluids* **16**, 17–26.

PEARSON, B. R. & ANTONIA, R. A. 1997 Velocity structure functions in a turbulent plane jet. *Proc. Eleventh Turbulent Shear Flow Conf., Grenoble*, pp. 3-117–3-121.

PRASKOVSKY, A. & ONCLEY, S. 1994*a* Measurements of the Kolmogorov constant and intermittency exponent at very high Reynolds numbers. *Phys. Fluids* **6**, 2886–2888.

PRASKOVSKY, A. & ONCLEY, S. 1994*b* Correlators of velocity differences and energy dissipation at very high Reynolds numbers. *Europhys. Lett.* **28**, 635–640.

SADDOUGHI, S. G. & VEERAVALLI, S. V. 1994 Local isotropy in turbulent boundary layers at high Reynolds number. *J. Fluid Mech.* **268**, 333–372.

SHAFI, H. S., ZHU, Y. & ANTONIA, R. A. 1996 Intermittency of vorticity in a turbulent shear flow. *Phys. Fluids* **8**, 2245–2247.

SHE, S. Z. & LEVEQUE, E. 1994 Universal scaling laws in fully developed turbulence. *Phys. Rev. Lett.* **72**, 336–339.

SIGGIA, E. D. 1981 Invariants for the one-point vorticity and strain rate correlation functions. *Phys. Fluids* **24**, 1934–1936.

SREENIVASAN, K. R. 1995 On the universality of the Kolmogorov constant. *Phys. Fluids* **7**, 2778–2784.

SREENIVASAN, K. R. & ANTONIA, R. A. 1997 The phenomenology of small-scale turbulence. *Ann. Rev. Fluid Mech.* **29**, 435–473.

SREENIVASAN, K. R. & KAILASNATH, P. 1993 An update on the intermittency exponent in turbulence. *Phys. Fluids* A **5**, 512–514.

STOLOVITZKY, G., SREENIVASAN, K. R. & JUNEJA, A. 1993 Scaling functions and scaling exponents in turbulence. *Phys. Rev.* E **48**, R3217–R3220.

TATARSKII, V. I. 1971 *The Effects of the Turbulent Atmosphere on Wave Propagation*. Keter Press.

TSINOBER, A., KIT, E. & DRACOS, T. 1992 Experimental investigation of the field of velocity gradients in turbulent flows. *J. Fluid Mech.* **242**, 169–192.

VAN ATTA, C. W. 1991 Local isotropy of the smallest scales of turbulent scalar and velocity fields. *Proc. R. Soc. Lond.* A **434**, 139–147.

VAN ATTA, C. W. & YEH, T. T. 1975 Evidence for scale similarity of intermittency in turbulent flows at large Reynolds numbers. *J. Fluid Mech.* **71**, 417–440.

VINCENT, A. & MENEGUZZI, M. 1991 The spatial structure and statistical properties of homogeneous turbulence. *J. Fluid Mech.* **225**, 1–20.

VUKOSLAVCEVIC, P. & WALLACE, J. M. 1981 Influence of velocity gradients on measurements of velocity and streamwise vorticity with hot-wire X-array probes. *Rev. Sci. Instrum.* **52**, 869–879.

YAGLOM, A. M. 1981 Laws of small-scale turbulence in atmosphere and ocean (in commemoration of the 40th anniversary of the theory of locally isotropic turbulence). *Izv. Atmos. Oceanic Phys.* **17**, 919–935.

ZHU, Y. & ANTONIA, R. A. 1995 Effect of wire separation on X-probe measurements in a turbulent flow. *J. Fluid Mech.* **287**, 199–223.